ELSEVIER

Journal of Nuclear Materials 254 (1998) 87–121

journal of nuclear materials

Review

A review of the oxidation of uranium dioxide at temperatures below 400°C

R.J. McEachern *, P. Taylor

Atomic Energy of Canada Limited, Whiteshell Laboratories, Pinawa, Man., Canada R0E 1L0

Received 17 January 1997; accepted 29 October 1997

Abstract

A critical review of the extensive literature on the air oxidation of UO_2 at temperatures below 400°C is presented. The key parameters that affect the rate of UO_2 oxidation are examined systematically and their importance to the reaction rate is evaluated. The formation of U_3O_7/U_4O_9 on unirradiated UO_2 powders follows the discrete-layer mechanism and displays diffusion-controlled kinetics. In contrast, U_3O_8 formation on unirradiated UO_2 displays sigmoidal 'nucleation-and-growth' kinetics. Low-temperature oxidation of used fuel tends to proceed by rapid grain-boundary oxidation followed by simultaneous intragranular oxidation throughout the sample. The best estimates of the activation energy for the formation of U_3O_7/U_4O_9 are 95.7 kJ mol^{-1} for UO_2 powders, 98.6 kJ mol^{-1} for sintered pellets and $\sim$106 kJ mol^{-1} for used fuel. The activation energy for the formation of U_3O_8 is temperature dependent. The best estimate of the activation energy below $\sim$325°C is 154 kJ mol^{-1}, but all the kinetic data incorporate substantial approximations so that further study is required to properly predict the behaviour of used fuel under low-temperature ($<$150°C) dry-air storage conditions, based on high-temperature (200 to 350°C) laboratory data. © 1998 Elsevier Science B.V.

1. Introduction

The stepwise oxidation of UO_2 in air to form U_3O_7 and U_3O_8 has been studied extensively for about 40 years [1–7], because of its relevance to the dry storage and the ultimate disposal of used [1] nuclear fuel [8–16], as well as UO_2 powder storage [2] and some fuel-recycling processes [17]. Nevertheless, many important aspects of the oxidation process are not yet fully understood. In particular, there are significant differences in oxidation behaviour between unirradiated UO_2 and used fuel [18–23], which have not been fully explained.

The oxidation of UO_2 is a two-step reaction [3]:

$$UO_2 \rightarrow U_3O_7/U_4O_9 \rightarrow U_3O_8. \quad (1)$$

The uranium dioxide starting material adopts the fluorite (CaF_2) type of crystal structure. The intermediate oxidation products, U_4O_9 and U_3O_7, are derivatives of this structure in which clusters of interstitial oxygen atoms are centred on unoccupied cubic sites in the fluorite-type lattice, with accompanying displacement of neighboring U atoms [24,25]. Formation of U_3O_7/U_4O_9 from UO_2 involves a slight volume reduction. In contrast, U_3O_8 has a distinctly different crystal structure [26] and a density that is 23% less than that of UO_2, which corresponds to a 36% net volume increase based on X-ray crystallographic densities [2]. Thus, the formation of U_3O_8 in a defective [3] fuel

* Corresponding author. Present address: PCS Inc., Allan Division, Allan, Sask., Canada S0K 0C0. Tel.: +1-306 257 3312.

[1] The term 'used fuel' denotes fuel that has been irradiated in a power reactor and is synonymous with 'spent fuel'.

[2] This corresponds to a ratio of 1.36:1 between the crystallographic volumes per uranium atom in U_3O_8 and UO_2 [27].

[3] The term 'defective', as opposed to 'intact', denotes fuel with a puncture in the cladding.

PII S0022-3115(97)00343-7

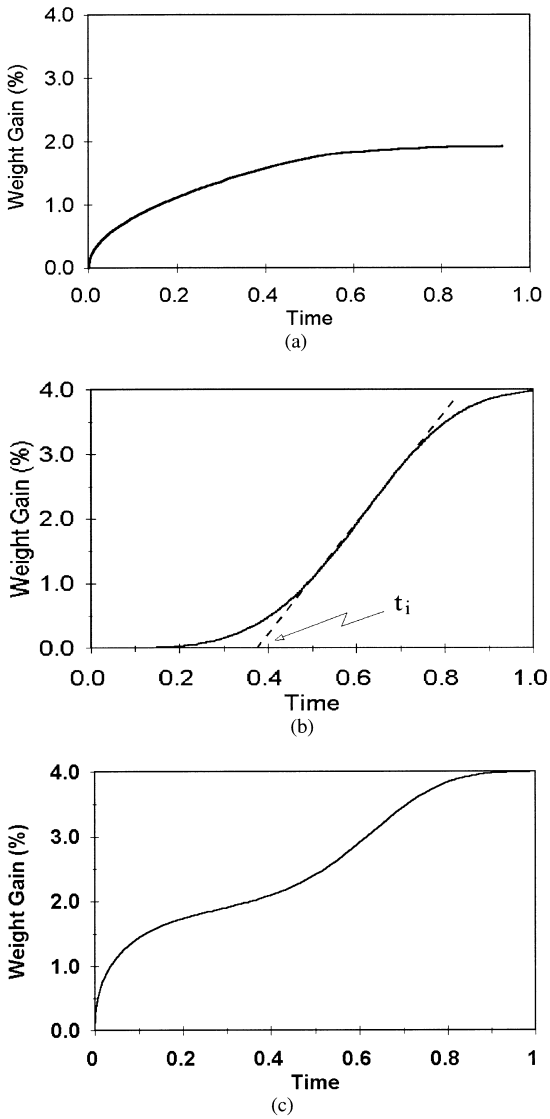

Fig. 1. Generalized reaction curves for the oxidation of UO_2. (a) Diffusion-controlled kinetics for the formation of U_3O_7/U_4O_9; (b) sigmoidal nucleation-and-growth kinetics for the formation of U_3O_8 and (c) overlapping formation of U_3O_7/U_4O_9 and U_3O_8, as commonly observed for UO_2 powders.

element can lead to splitting of the sheath [23,28–30], which can complicate subsequent handling and disposal of the fuel [4]. A detailed knowledge of the kinetics and mechanism of U_3O_8 formation is needed to define acceptable upper temperature limits for air storage of used nuclear fuel [8,32].

The air oxidation of UO_2 is complicated because the reaction has two stages (Eq. (1)), which have different reaction mechanisms and which often occur concurrently (Fig. 1). The intermediate U_3O_7/U_4O_9 forms as a discrete layer on the surface of the UO_2 sample [12], and the rate of oxidation is generally limited by the rate of oxygen diffusion through the U_3O_7/U_4O_9 product layer. The rate of U_3O_7/U_4O_9 formation is thus proportional to the square root of time, i.e. parabolic reaction kinetics are observed [1,4,33,34].

The formation of U_3O_8 follows a nucleation-and-growth mechanism [1] and, therefore, displays sigmoidal reaction kinetics [28,35–37] as shown in Fig. 1. The initial rate of oxidation is very low (the 'induction period') followed by a gradually increasing oxidation rate up to a maximum (sometimes called the linear region) that then tails off as the reaction approaches completion. The rate of formation of U_3O_8 is generally modelled with nucleation-and-growth expressions, such as those of Johnson and Mehl [38,39] and Avrami [40] and Erofeev [41]. The rate of reaction has also been reported in terms of the pseudo-linear region near the mid-point of the reaction [42].

The U_3O_8 that forms on a sintered UO_2 sample generally spalls from the surface as a fine powder [10,17]. In a UO_2 oxidation experiment, the time required for visual observation of U_3O_8 powder is referred to as the powder-formation time, t_p [43]. A related parameter, the induction time (t_i) is defined as the x-axis intercept of the line that approximates the maximum, 'linear' rate portion of the sigmoidal reaction curve, Fig. 1(b) [42]. In some cases, such as the oxidation of sintered pellets, the description of U_3O_8-formation kinetics with a linear model may be appropriate, because the rate of oxidation can be limited by

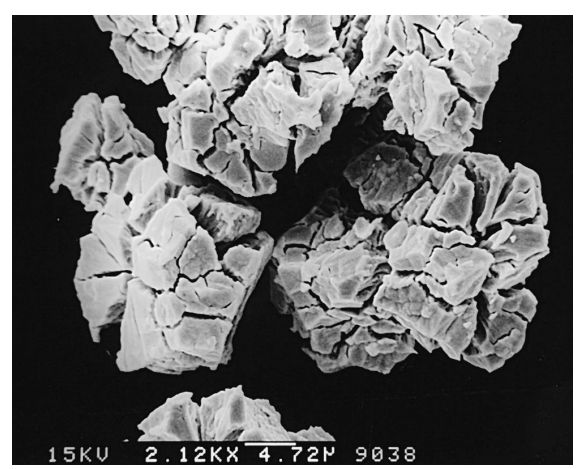

Fig. 2. Scanning electron micrograph of U_3O_8 powder prepared by oxidizing UO_2 fuel in air at 400°C for 16 h, showing the 'popcorn' morphology arising from the 36% volume expansion associated with the conversion.

[4] The integrity of intact fuel elements is limited by cladding degradation mechanisms, such as stress-corrosion cracking, rather than UO_2 oxidation [31].

Table 1
Glossary of technical terms and acronyms

AGR	advanced gas-cooled reactor
D^O	chemical diffusion coefficient of oxygen in UO_{2+x}
DS	dehydrated schoepite, $UO_3 \cdot xH_2O$, $x \sim 0.7$ to 0.9, this phase has a crystal structure closely related to α-$UO_2(OH)_2$
LWR	light-water reactor; includes boiling water reactor (BWR) and pressurized water reactor (PWR)
O/M	oxygen:metal mole ratio
PNL	Pacific Northwest Laboratories
REE	rare earth (element)
RH	relative humidity
SEM	scanning electron microscopy
TD	theoretical density
t_i	induction time
t_p	time-to-powder
XRD	X-ray diffraction (usually powder diffraction)
XPS	X-ray photoelectron spectroscopy

Table 2
Conversion factors for various burnup units

1 MW h = 3.6 GJ
1 MW d = 86.4 GJ
1 MW a = 31.6 TJ
1 MW/kg = 1 GW/t
1 at.% ≈ 225 MW h/kg U, depending on the type of fuel and the stage of burnup

the rate of cracking and spalling of the U_3O_8 product [9,17,42].

The spalling of oxide powder from UO_2 pellets is evidently a result of the volume expansion associated with the conversion to U_3O_8 (see above). Microscopic examination of the powder typically shows particles the size of original UO_2 grains, or fragments thereof, which are often highly fractured, displaying a 'popcorn' or 'cauliflower' appearance, as shown in Fig. 2. Most of the expansion takes place in the [111] crystallographic directions of the UO_2 precursor (see Sections 2.1 and 2.8.4.2). There are eight such, equivalent directions in a UO_2 grain (along the body diagonals of the cubic structure). We suggest that the fractured, popcorn morphology arises from tensile forces generated within a grain in which different regions (sub-grains) are expanding simultaneously in several of these equivalent directions (i.e. the growing U_3O_8 is twinned; see Section 2.1). Sub-micrometre sized particles of UO_2 appear to be sufficiently small to withstand expansion without cracking, perhaps because they normally generate only one U_3O_8 nucleus per prior UO_2 grain, or because the tensile strains are proportional to grain size.

The low-temperature (i.e. $< 250°C$) oxidation of unirradiated fuel, or UO_2 doped with only low concentrations of impurities (to simulate low-burnup used fuel), yields U_3O_7 [44,45] or similar phases that have tetragonal (or at least, non-cubic) symmetry. Oxidation of used CANDU® [5] fuel, with burnups typically in the range 6 to 12 MW d/kg U, sometimes results in the formation of a phase resembling U_3O_7 and sometimes a cubic phase resembling γ-U_4O_9 [16]. Oxidation of used LWR fuel (typical burnups 20 to 50 MW d/kg U) or UO_2 doped with large amounts (≥ 4 at.% [6]) of impurities results exclusively in the formation of a cubic phase resembling γ-U_4O_9 [45]. In situations where the crystallographic distinction is not made, we commonly use the term U_3O_7/U_4O_9 to represent intermediate oxidation products of this type. We include only a limited discussion of the crystallographic nuances of the U_3O_7/U_4O_9 group of phases (Section 3.1); these aspects have been addressed in detail by several authors, including Belbeoch et al. [46], Hoekstra et al. [6] and Ohashi et al. [7]. A useful compilation of XRD data for U_3O_7/U_4O_9, U_3O_8 and other phases in the U–O–H_2O system, is presented by Thomas et al. [47].

From the practical viewpoint of fuel storage, the most important aspect of the air oxidation of used fuel is the rate of production of U_3O_8 as a function of time, temperature, burnup and other physical parameters. In this review, we examine the factors that affect the oxidation process, as well as the underlying reaction mechanism. Because of their practical importance, we pay particular attention to the kinetics and mechanism of U_3O_8 formation, as well as the differences in oxidation behaviour between UO_2 and used fuel. A glossary of technical terms and acronyms is provided in Table 1 and a list of conversion factors for various burnup units is given in Table 2.

2. Parameters that affect the rate of UO_2 oxidation

In this section, we review the literature on the qualitative effects of those parameters that have an important impact on UO_2 oxidation, to draw conclusions where possible and to identify areas where further research is needed. Quantitative aspects of the rate of formation of U_3O_7/U_4O_9 and U_3O_8 are discussed in the sections on activation energies (Sections 3.5 and 3.6).

2.1. Temperature

The thermodynamically stable product of UO_2 oxidation in dry air below about 700°C is γ-UO_3 [48–50]. In

[5] CANDU® is a registered trademark of Atomic Energy of Canada Limited (AECL).

[6] Throughout this report the term at.% refers to the fraction of the total metal content on an oxygen-free basis.

practice, however, air oxidation of UO_2 does not proceed beyond U_3O_8 [7]. Oxidation of UO_2 is a complex, kinetically controlled process, the extent of which depends on time, temperature and the oxygen potential of the atmosphere (for a discussion of the latter, see Section 2.4).

The chemisorption of molecular oxygen onto the surface of UO_2 is the first stage of the oxidation reaction. Roberts [51] found that chemisorption occurs rapidly on the surface of UO_2, even at temperatures as low as -183°C, and concluded that the activation energy for this process is extremely low. He also reported that at least half the U^{4+} ions on the UO_2 surface are involved in the chemisorption of oxygen. Ferguson and McConnell [52] reported that the heat of chemisorption is about -230 kJ mol^{-1} during the initial stages of the reaction, declining to about -20 kJ mol^{-1} in the later stages. This highly exothermic process helps to account for the observation that freshly reduced, finely powdered UO_2 can be pyrophoric [2,3,53].

At higher temperatures (-130 to $+50$°C) powdered UO_2 undergoes further reaction with the formation of an oxidized layer, typically a few nanometres thick. At 20°C, extremely fine UO_2 powders (~ 50 nm particle diameter) oxidized up to a bulk composition of $UO_{2.16}$ to $UO_{2.18}$; this corresponds to an oxidized (U_4O_9) layer thickness of about 5 nm [54]. The XRD analysis of such powders revealed that they were similar to large-particle-size powders oxidized at higher temperatures. In these experiments, care was needed to avoid over-oxidation by self-heating, therefore samples were pre-oxidized at -78°C. Kinetic data were obtained with coarser powders (0.4 to 2.3 μm particle diameter); Anderson et al. [53,54] and Roberts [55] found that the degree of oxidation in this temperature range was proportional to the logarithm of time.

The authors concluded that oxidation at low (-130 to $+50$°C) temperatures yields products similar to those obtained at high temperature but that they are limited to a thin surface layer, because bulk diffusion of oxygen ions is extremely slow below ~ 50°C. They proposed a mechanism similar to that used to explain the formation of thin oxide films on metals at temperatures too low for normal diffusion-based processes [54]. In such reactions, metal diffusion is driven by the high electrostatic field generated between the metal and adsorbed oxygen ions [56].

At temperatures above about 100°C, the rate of oxygen diffusion is rapid enough that bulk oxidation to U_3O_7/U_4O_9 can be measured [4,35,53]. The oxidation of powders to U_3O_7/U_4O_9 is observed between 100 and 250°C [4,53], whereas at higher temperatures it occurs concurrently with the formation of U_3O_8. Oxidation of sintered pellets does not generally yield pure U_3O_7/U_4O_9 because U_3O_8 formation typically begins while the U_3O_7/U_4O_9 product layer is only a few micrometres thick. However, the formation of discrete layers of U_3O_7/U_4O_9 on fuel pellets is readily observed by XRD [4,44,57], electron microscopy [12,58] or X-ray photoelectron spectroscopy (XPS) [57,59,60].

The rate of chemical diffusion of oxygen in UO_{2+x} is an important phenomenon in the study of UO_2 oxidation because the first stage of the oxidation reaction is diffusion controlled. The kinetics of oxygen chemical diffusion in UO_{2+x} have been studied extensively and the results have been reasonably consistent in the range 500 to 1400°C [61]. Matzke (fig. 20 of Ref. [61]) showed that the chemical diffusion coefficient of oxygen (D^O) in UO_{2+x} is quite insensitive to x, with a value of $D^O \sim 1.5 \times 10^{-7}$ $cm^2\ s^{-1}$ at 1000 K. Similarly, the activation enthalpy for D^O has been estimated at 96 ± 8 kJ mol^{-1}. Thus, it is possible to estimate the diffusion coefficient, D^O as a function of temperature:

$$D^O = D^O_{1000} e^{\{(E_a/1000R) - (E_a/RT)\}}, \quad (2)$$

$$D^O = (1.5 \times 10^{-7}\ cm^2\ s^{-1}) e^{(11.57 - (1.157 \times 10^4/T))}. \quad (3)$$

The chemical diffusion coefficients obtained with Eq. (3) are reasonably consistent with data available from reported oxidation experiments. For example, Aronson et al. [1] measured chemical diffusion coefficients for the formation of U_3O_7 on fine UO_2 powders and derived an Arrhenius expression for D^O which gives a value of 9.8×10^{-9} $cm^2\ s^{-1}$ for 1000 K. The data provided by Aronson et al. [1] are typical of the many reports of kinetic data for the first stage of UO_2 oxidation, as reviewed by McEachern [62].

Above 250°C, bulk oxidation to the orthorhombic U_3O_8 phase occurs at an easily measurable rate. This reaction is known to follow sigmoidal nucleation-and-growth kinetics [1]. The rate of nucleation depends on many factors and, thus, there is a wide range in the reported rates of U_3O_8 formation. Nucleation is rapid on powdered materials, so that for example, U_3O_8 is observed as a major product on powdered UO_2 at 260°C after ~ 25 h [1], whereas a comparable degree of oxidation is restricted to the surface of sintered pellets after ~ 100 h [10]. Moreover, on sintered pellets there is a wide range in the rate of nucleation, because U_3O_8 nuclei form faster on rough surfaces than on polished specimens [10,57]. The formation of U_3O_8 leads to spallation of oxidized product, thereby exposing the underlying UO_2 to the oxidizing atmosphere. Linear kinetics are observed during the U_3O_8 formation/spallation stage of the oxidation process, until the reaction slows down as it approaches completion [9,42,63].

The exact nature of the U_3O_8 nucleation process is not understood. The crystal structure of U_3O_8 is markedly different from the fluorite structure of UO_2 and its deriva-

[7] This is presumably due to a large energy barrier for γ-UO_3 nucleation on U_3O_8, but one can only speculate on the structural reasons.

tives of the U_3O_7/U_4O_9 type [26]. Allen et al. [64] have pointed out that the net crystallographic change between the fluorite structure and U_3O_8 can be described in terms of a uniaxial expansion of the uranium sublattice in the [111] direction of the fluorite structure. This is accompanied by a major reorganization and expansion of the oxygen sublattice. Such a dramatic structural change is expected to be initiated at specific points (nucleation sites) on the oxide surface, determined by factors such as surface topography (roughness), crystallographic orientation and the presence of structural defects or dislocations. The crystallographic relationship between U_3O_8 and the fluorite structure is discussed further in Section 2.8.4.2.

Above $\sim$350°C the intermediate U_3O_7/U_4O_9 is generally not observed in major quantities; instead, the bulk oxidation appears to proceed directly to U_3O_8 [35]. Above $\sim$500°C the rate of U_3O_8 formation on sintered UO_2 pellets does not display Arrhenius behaviour, but rather, it declines with increasing temperature [42,65,66]. This behaviour has been attributed to the increased plasticity of U_3O_8 above 500°C; thus, the U_3O_8 formed does not readily spall from the UO_2 surface but instead forms a barrier to retard further oxidation [66,67]. The particle size of U_3O_8 powder generated by air oxidation of UO_2 pellets increases with oxidation temperature [68], perhaps because of increasing U_3O_8 plasticity between 400 and 700°C.

The major product of UO_2 oxidation remains U_3O_8 up to $\sim$1100°C, above which U_3O_8 decomposes (at atmospheric pressure) to a series of oxides with slightly lower O:U ratios and above 1500°C these decompose to UO_{2+x} [49]. These high-temperature reactions are beyond the scope of the present review.

2.2. Moisture

The addition of water to the UO_2–O_2 system complicates the chemistry of UO_2 oxidation [50,69]. At atmospheric pressure, in the absence of oxygen or other gas-phase oxidants, high-temperature steam does not oxidize UO_2 beyond the fluorite-type UO_{2+x} phase, whereas higher oxides can be formed at elevated pressures, e.g. up to $O/U = 2.60$ at 1600 K and 15 MPa pressure [67,70]. At lower temperatures, water can influence the air oxidation of UO_2 in several ways. As an additional chemical component, it introduces the possibility of forming hydrated oxidation products, such as schoepite ($UO_3 \cdot 2H_2O$) and other UO_3–H_2O compounds [27,50,71,72]. As a reaction medium (either bulk liquid or condensed film), it allows oxidation to proceed by dissolution–precipitation as well as solid-state mechanisms [27,50,71–73]. Moisture may also enhance oxygen diffusion along grain boundaries in sintered UO_2 pellets [16]. Finally, in the case of used fuel, water is a potential source of radiolytic oxidation products, such as hydrogen peroxide and various free radicals, which may alter both the kinetics and the products of oxidation [16].

The effect of water vapour on UO_2 oxidation depends on the moisture content (i.e. the relative humidity, RH) of the oxidizing atmosphere. If any water is present in the oxidizing atmosphere, a hydroxylated surface layer (chemisorbed water) is likely to be formed; this is a common feature of oxide surfaces [74–76]. For example, analysis by XPS of unirradiated UO_2 specimens that had been oxidized in ambient air (150 to 270°C), yielded evidence of a monomolecular surface layer of hydroxyl ions [57,59,77,78]. We are not aware of any evidence that other components of air, such as CO_2, influence the oxidation mechanism.

At RH < 40%, the bulk products of UO_2 oxidation are the same as for dry-air oxidation, i.e. U_3O_7/U_4O_9 and U_3O_8 [71]. In contrast, reactions at RH > 40% or in aerated water yielded mixtures of U_3O_8 and dehydrated schoepite (DS) [8] [27,50,71–73]. The relative proportions of U_3O_8 and DS formed under such moist conditions depend on the oxidation time and the oxygen content of the system, but a detailed interpretation is difficult to achieve because of generally poor experimental reproducibility [71]. This is attributable partly to sample variability and partly to the complexity of competing precipitation reactions. The microstructure of the oxidation products varies with relative humidity, from scattered crystals at RH $\sim$ 40% to textured layers at RH $\sim$ 60–80% and thicker, microcrystalline layers at RH values just below saturation [73]. Above saturation, large crystals of DS, along with finer-grained U_3O_8, are able to grow from bulk solution [72,83]. When the oxygen supply is depleted, back-reduction of DS to U_3O_8 may also occur on a UO_2/U_3O_7 surface [72], because U_3O_8 is marginally stable with respect to the hydrous disproportionation reaction [50]:

$$2U_3O_8(s) + 3xH_2O(l) \rightarrow U_3O_7(s) + 3UO_3 \cdot xH_2O(s). \quad (4)$$

The Gibbs energy change for Eq. (4) has been calculated for $x = 0.9$ (i.e. dehydrated schoepite); it increases from $+13.5$ kJ mol^{-1} at 25°C to $+42.9$ kJ mol^{-1} at 225°C, i.e. from $+2$ to $+7$ kJ/mol U [72].

Early work on the effect of relative humidity on the rate of UO_2 oxidation (Eq. (1)) was inconclusive, with some workers reporting a slight increase in the rate with increasing moisture content [84,85] and others detecting no effect [86,87]. Taylor et al. [71] oxidized slices of unirradiated CANDU fuel pellets in dry, moist and wet air at 200 to 225°C. They did not make quantitative comparisons between the rate of oxidation under moist and dry conditions; however, the effect of moisture, if any, appeared to be minor, and was swamped by the high degree of variabil-

[8] For a description of the preparation and properties of dehydrated schoepite and other UO_3–H_2O phases, see Refs. [79–82].

ity in the depth of intergranular attack between different specimens, even when they were obtained from the same UO_2 fuel pellet. Weight-gain experiments performed at Pacific Northwest Laboratories have shown that there is a small but significant increase in the rate of oxidation of unirradiated UO_2 pellets with increasing moisture content of the oxidizing atmosphere [19,43,88].

Surface oxidation of UO_2 samples has likely contributed to at least some of the ambiguities over the effect of moisture levels on the rate of air oxidation of UO_2 since the formation of a surface layer of UO_3 (or hydrates thereof) can have a significant impact on weight-gain experiments. It is well established that UO_3 is stable with respect to U_3O_8, at any measurable oxygen concentration and temperatures relevant to dry air storage, i.e. < 200°C [48,50,69,71]. Also, the formation of UO_3 hydrates is thermodynamically favourable in the presence of significant quantities of moisture [50]. The lack of formation of bulk quantities of UO_3 or its hydrates is thus presumably related to kinetic rather than thermodynamic factors. Nevertheless, there is ample evidence for the formation of UO_3 (or UO_3 hydrates) on the surface of UO_2 samples. Wang [89] reported that a thin (~ 20 Å) layer of UO_3 hydrate was formed on the surface of single-crystal UO_2 when air-oxidized for 24 h at 285°C. Wadsten [90] stored UO_2 powder in ambient air for 15 years and found by XRD analysis that small amounts of $UO_3 \cdot 2H_2O$ were formed. Similarly, Hoekstra et al. [6] oxidized UO_2 powders with high surface area (30 $m^2\ g^{-1}$) at 25°C and found that the infrared spectrum of the product resembled that of amorphous UO_3. Therefore, the high weight gains observed in some air oxidation tests using fine UO_2 powder may have resulted from the formation of a surface layer of UO_3 or one of its hydrates.

On balance, the data appear to suggest that moisture has a small, but significant impact on the rate of oxidation of unirradiated fuel pellets [19,43,88]. Conversely, numerous tests on used fuel (fragments, coarse powders and microspheres) have shown that humidity (RH $\leq 33\%$) has no effect on the rate of oxidation [5,45,91,92] or even that increasing humidity diminishes the oxidation rate slightly [93].

Perhaps some of the differences in moist-oxidation behaviour between unirradiated UO_2 and used LWR fuel can be explained in terms of the grain-boundary oxidation process. In used LWR fuel, oxygen diffusion along grain boundaries is rapid because of fission-gas bubbles and microscopic defects. Thus oxidation of used LWR fuel to U_4O_{9+y} can be considered to proceed simultaneously throughout the sample, along the grain boundaries and into the UO_2 grains. In such a case the presence of adsorbed moisture is unlikely to accelerate the oxidation process. In contrast, it is possible that the rate of oxidation of unirradiated fuel may be faster in the presence of significant amounts of moisture, because the oxidation does not occur simultaneously throughout the sample. Rather, grain-boundary oxidation is relatively slow, so that oxidation proceeds via an oxidation front [44,57]. In this case, moisture may speed up the reaction by selectively hydrolysing U–O–U bonds at the grain boundaries, thus enhancing access of oxygen to the grain boundaries and thence to the interior of the sample.

The effect of moisture on the air oxidation of used CANDU fuel has also been examined. High-moisture (100% RH), limited-air tests were performed on used CANDU fuel at 150°C and it was found that the presence of moisture greatly enhanced the extent of grain-boundary oxidation, as compared with dry air oxidation [94]. In the high-moisture tests, a thin layer of highly oxidized material appears to have formed along grain boundaries and in regions of the fuel with high porosity. Wasywich et al. [16] suggested that radiolytic processes may have played a role in the oxidation behaviour of this material, because the pH of the storage water in some experiments was found to be as low at 1.55 combined with 1920 ppm NO_3^- [95]. The findings of Wasywich et al. [16] should be interpreted with caution because the air supply in their experiments was limited. Clearly, the oxidation reactions of used fuel under such low-temperature, high-humidity conditions is a complex field that merits further study.

2.3. Dopants

The effect of dopants on the UO_2 oxidation process has been studied for many years [63,96–101], because of the significant amounts of fission-product impurities present as a solid solution in used fuel, e.g. ~ 1 at.% fission products are found in fuel for each 10 MW d/kg U of burnup [102]. Impurity elements are also important in the chemistry of uraninite, an impure natural form of UO_2, for which Janeczek and Ewing [103] have proposed the structural formula: $(U^{4+}_{1-x-y-z}U^{6+}_{x}REE^{3+}_{y}D^{2+}_{z})O_{2+x-0.5y-z}$, where REE represents rare-earth elements and D^{2+} represents a divalent impurity such as Ca^{2+} or Pb^{2+}.

Some thermodynamic information on the effect of impurities (M) on the oxidation of UO_2 is contained in the ternary U–M–O phase diagrams. These phase diagrams are generally well established for M = Th, Pu, rare earths and many other elements; the results are described in a number of review articles [104–108]. Here, we are mainly concerned with the properties of UO_2 that relate to the oxidation of used fuel and we thus focus on the behaviour of UO_2 doped with low concentrations of impurities.

One of the most prominent properties of doped UO_2 is the enhanced kinetic stability (relative to pure uranium oxides) of the cubic U_4O_{9+y}-type structure with respect to U_3O_8 formation. Oxidation experiments performed on doped UO_2 show that it commonly retains the fluorite structure to higher temperatures, and for longer times, than the undoped material [45]. Because of their relevance to the nuclear industry, the effect of impurity ions such as Pu^{3+} and Pu^{4+}, REE^{3+} and Th^{4+} on the stability of the

fluorite phase has been studied extensively. The effect on oxidation of other ions, such as Mg^{2+}, Ca^{2+}, Al^{3+}, Ti^{4+}, V^{5+} and Mo^{6+} has also been examined [109].

The importance of (U, Pu)O_2 as a reactor fuel led to the study of the effect of Pu^{3+} on the rate of UO_2 oxidation. Rouault and Girardin [110] oxidized UO_2 pellets and $(U_{0.86}Pu_{0.14})O_2$ at 450°C in an atmosphere of O_2 (2%) in nitrogen. They found that the UO_2 pellet was completely powdered after 22 h, whereas the (U, Pu)O_2 pellet was only beginning to powder after 24 h. Similarly, they noted that for oxidation of (U, Pu)O_2 at 600°C, the quantity of U_3O_8 formed was inversely related to the plutonium content and that no U_3O_8 was formed for material with >20 at.% Pu after heating 150 h. Tennery and Godfrey [111] obtained qualitatively similar results. They oxidized $(U_{0.8}Pu_{0.2})O_2$ in air at 450 to 600°C and found that a mixture of M_3O_8 and a cubic phase were formed. In contrast, when they oxidized $(U_{0.75}Pu_{0.25})O_2$ they found that only a face-centred cubic phase, $M_4O_{9.4}$, was formed, even when the material was heated up to 800°C. We thus conclude that the presence of plutonium in UO_2 fuel retards the formation of U_3O_8; however, quantitative analysis of the effect of plutonium has not yet been studied. Such analysis may be difficult because (U,Pu)O_2 is often inhomogeneous [112].

Because the 4+ oxidation state of thorium is very stable, it is not surprising that $Th_yU_{1-y}O_2$ solid solutions are more oxidation-resistant than pure UO_2. The resistance to U_3O_8 formation increases with thorium content, so that materials with $y>0.2$ retain the fluorite structure at least up to 1400°C [96], and materials with $y>0.5$ are stable under highly oxidizing conditions [96,113,114].

The effect of REE and other trivalent ions, such as Y^{3+}, on the high-temperature oxidation of UO_2 has also been studied [101,114]. Wilson et al. [101] noted increased resistance to oxidation with increasing amounts of M_2O_3 in solid solution with UO_2 when oxidized in air in the range 1375 to 1750°C. Thomas et al. [45] compared the oxidation at lower temperatures (<600°C) of pure UO_2 with doped materials containing 4 and 8 wt% Gd_2O_3 as well as 0.4 wt% NbO_2, using thermal analysis and XRD. They found that with each type of material the eventual product of oxidation was U_3O_8 but that increasing dopant levels led to the formation of U_3O_8 at higher temperatures and weight gains. Analysis of partially oxidized material (oxidized to the same degree of weight gain) revealed higher amounts of U_3O_8 in the material doped with lower amounts of impurities. Campbell et al. [43] also found that the presence of gadolinium (5 and 10%) in UO_2 inhibited the formation of U_3O_8 when oxidized at 200°C. Kim et al. [22] recently provided an eloquent introduction to UO_2-oxidation chemistry, together with new data on the oxidation of irradiated, Gd-doped UO_2 fuel; their results were comparable to those of Campbell et al. [43].

The slow rate of U_3O_8 formation in doped UO_2 results in longer induction times for U_3O_8 powder formation than for undoped material [22,43], indicating that impurities may affect the U_3O_8 nucleation and growth processes. The observed correlation between the time to [U_3O_8] powder formation (t_p) and burnup [18–20,115,116] is likely related to the large amount of fission-product dopants in high-burnup fuel. Such a conclusion is supported by the fact that Choi et al. [117] were able to replicate the burnup dependence of t_p using simulated used fuel (SIMFUEL), which has the fission-product content of used fuel [118].

Low-temperature oxidation tests have shown that the onset of U_3O_8 formation occurs at larger weight gains in the oxidation of doped UO_2 than undoped material [43,45]. The weight-gain data obtained by Thomas et al. [45] with gadolinium-doped UO_2 indicated that the resulting U_4O_{9+y} had the composition (U, Gd)$O_{2.4}$, which is more oxygen-rich than U_3O_7 ($UO_{2.33}$). Similar results have been obtained for UO_2 doped with plutonium [111] or thorium [119] and for used LWR fuel [120]. It has been suggested that the high O/M ratio in such samples is a possible reason for the observed direct transformation from U_4O_{9+y} to U_3O_8 [45].

The stability of the cubic fluorite phase in doped UO_2 is enhanced relative to the undoped material, so that there is a qualitative change in the nature of the oxidation mechanism; i.e. the intermediate U_4O_{9+y} is observed rather than U_3O_7. Thomas et al. [45] and Campbell et al. [43] oxidized UO_2 and gadolinium-doped UO_2 samples at low (175 to 200°C) temperatures. Measurement of the XRD patterns of partially oxidized samples indicated that oxidation of pure UO_2 (or UO_2 doped with low amounts of impurities) proceeds via U_3O_7, whereas UO_2 doped with large amounts (4 to 10 wt%) of Gd_2O_3 oxidized via U_4O_{9+y}. Janeczek et al. [121] reported that uraninite and pitchblende samples, each of which had considerable levels of impurities (up to 20 wt% Ca, Pb, REE, etc.) oxidized to cubic U_4O_9-type structures at 300°C. Similar results have been observed with plutonium-doped material; oxidation of $(U_{1-x}Pu_x)O_2$ with $x<0.2$ leads to the formation of an intermediate tetragonal M_3O_7 phase, whereas material with a higher plutonium content retains a cubic structure [111,114,122]. The low-temperature (175 to 200°C) oxidation product of UO_2 doped with thorium (17 to 30 at.%) was found to retain cubic symmetry, even though comparable undoped samples were tetragonal [119]. The accepted oxidation sequence for UO_2 is thus

$$UO_2 \rightarrow U_3O_7 \rightarrow U_3O_8. \quad (5)$$

In contrast, oxidation of UO_2 doped with large amounts of impurities appears to proceed via the sequence

$$UO_2 \rightarrow U_4O_{9+y} \rightarrow U_3O_8. \quad (6)$$

The behaviour of highly doped UO_2 is clearly similar to that of used LWR fuel, because U_4O_{9+y} is also the observed intermediate product when used LWR fuel is

oxidized at low temperatures. Thomas et al. [45] noted that U_4O_{9+y} XRD peaks were less broad than the corresponding peaks observed in oxidized used fuel but that otherwise the patterns were similar. They found that the U_4O_{9+y} formed in used LWR fuel is similar to γ-U_4O_9 (which is normally stable only at elevated temperatures) rather than the long-range ordered β-U_4O_9 (stable at low temperatures). In contrast to the situation with LWR fuel, used CANDU fuel apparently oxidizes at low temperatures via the U_3O_7 intermediate [16]. Such a result is probably due to the lower burnup for CANDU fuels, which results in lower levels of fission-product impurities. This conclusion is supported by recent studies with simulated used fuel, SIMFUEL [117], which showed that the intermediate oxide was tetragonal with low simulated burnups and that there was a tendency to retain the cubic structure with increasing simulated burnup.

The appearance of the intermediate U_4O_{9+y} rather than U_3O_7 is indicative of enhanced stability of the cubic phase for the doped materials, perhaps because dopants disrupt the defect-cluster ordering that is thought to be responsible for the tetragonal distortion of the fluorite lattice in U_3O_7 (Thomas and Taylor, in preparation). However, the reasons for the stability of the fluorite phase in the doped materials remains unclear. Anderson et al. [96] suggested that the O/M limit of 2.34 observed for the oxidation of (U, Th)O_2 was related to the geometry of the crystal structure, i.e. to the ability to fit oxygen ions into interstitial sites. Janeczek et al. [121] described two possible mechanisms to account for the retention of cubic phases during uraninite oxidation. They suggested that thorium impurities in their uraninite sample inhibit deviation from cubic symmetry by limiting the number of oxygens that can fit into interstitials in the fluorite-type structure. They also suggested that radiation-induced point defects, such as oxygen interstitials, may inhibit oxidation by limiting the rate of oxygen diffusion into the lattice. However, since interstitials are the diffusing species that control the oxidation mechanism, it is difficult to visualize how their generation would inhibit oxidation.

In summary, the enhanced stability of doped UO_{2+x} and U_4O_{9+y}, relative to the analogous undoped structures, results in the retention of the cubic phases to higher temperatures, longer heating times and higher O/M ratios during oxidation experiments. Several ideas have been put forward to explain the stability of the cubic phases, but a detailed theoretical understanding has not yet been achieved. Ultimately, the stability of the doped material will need to be explained in terms of a model that takes into consideration the relative energy of various defects (impurity ions, interstitial oxygens, etc.) as well as the rates of diffusion and phase transformations. In particular, it would be interesting to estimate the effect of ions such as Th^{4+} and REE^{3+}, which are inert to oxidation, on the incorporation of interstitial oxygen ions into the lattice. Recent theoretical studies have made good progress towards describing the oxygen potential and other properties of UO_2 in terms of the defects therein [123–127], but further work will be required to explain completely the oxidation mechanism of doped UO_2.

2.4. Oxygen partial pressure

It has long been recognized that both the rate and extent of UO_2 oxidation depend on the oxygen partial pressure [128,129]. However, there is no simple relationship between oxidation rate and pressure, because the oxidation process changes qualitatively as a function of temperature (Section 2.1). In this section we examine the oxidation reaction at low (i.e. atmospheric and lower) pressures because this is the range of most relevance to fuel storage; the uranium–oxygen phase diagram at high temperatures and pressures has also been studied [130], but is not considered here.

2.4.1. Oxidation of UO_2 powders

One of the first stages of UO_2 oxidation is the rapid formation of a thin layer of oxidized product [3]. Anderson et al. [54] studied this process with UO_2 powders in the temperature range -130 to 50°C and estimated that the layer of oxidized product was ~ 5 nm thick, as discussed in Section 2.1. They found that the oxidation rate increases slightly with increasing pressure, however, they did not determine a quantitative relationship between pressure and oxidation rate for this temperature range.

At temperatures above 100°C, oxidation is sufficiently fast to be considered a bulk, rather than surface, process (see Section 2.1); the pressure dependence of the rate of bulk oxidation to U_3O_7 has also been examined. Anderson et al. [54] oxidized UO_2 powders in the range 130 to 180°C and found that the parabolic rate constant, k, for the formation of U_3O_7 is proportional to p^n, where p is the oxygen pressure and n varies between 0.13 and 0.16. They thus concluded that the surface adsorption of oxygen follows Freundlich isotherm behaviour. Further, they suggested that the observed rate of oxidation of UO_{2+x} decreases at low pressures because the concentration of 'mobile oxygen' (i.e. interstitial oxygen anions) at the surface is a function of pressure; they did not notice any systematic pressure dependence of the activation energy for the oxidation process. Blackburn et al. [4] measured the parabolic rate constant at 200°C for pressures between 0.07 and 101 kPa. Their data indicate that there is little change in oxidation rate between 20 and 101 kPa, but that at low oxygen pressures (< 20 kPa) the oxidation rate decreases; they suggested that the reduction in rate is probably due to the lack of adequate oxygen to saturate the outer layer of U_3O_7.

In Fig. 3, we compare the data reported by Anderson et al. [54] at 183°C and by Blackburn et al. [4] at 200°C. The data from Anderson et al. [54] were converted to parabolic rate constants ($cm^2\ s^{-1}$), to facilitate this comparison.

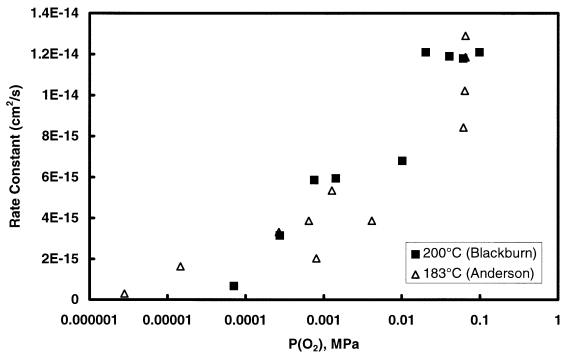

Fig. 3. Selected data showing the dependence of UO_2 oxidation rate on oxygen partial pressure. The parabolic rate constant is compared for data reported by: ■ Blackburn et al. [4] at 200°C; △ Anderson et al. [54] at 183°C.

There is good agreement on the magnitude of the overall pressure dependence (about a factor of 6 over the pressure range from 0.2 kPa to 0.1 Mpa). The apparent discrepancy in absolute rates (given the temperature differential between the two data sets) can probably be attributed to uncertainties in the surface-area measurements. Direct comparison with data for sintered pellets is difficult; the magnitude of pressure effects reported by Smith [63] at 300°C is similar to that depicted in Fig. 3, whereas Tucker et al. [42] did not observe a clear pressure dependence on the oxidation rate in the pre-induction period at temperatures above 225°C.

Vlasov and Bessonov [131] also found that the rate of U_3O_7 formation depends on pressure. They found that between 0.33 and 13.3 kPa the rate of oxidation is proportional to the pressure, whereas in the range 13.3 to 80 kPa the rate is proportional to the square root of pressure. Because their experiments, however, were performed at 340°C the results are probably not valid for the formation of U_3O_7 but rather for a combination of U_3O_7 and U_3O_8. Saito [132] reported that the rate of oxidation of UO_2 powders was independent of oxygen pressure at temperatures from 175 to 330°C and pressures between 2.5 and 101 kPa. These are higher temperatures and a more limited pressure range than those investigated by Anderson et al. [54] and Blackburn et al. [4]. Thus the pressure dependence of the oxidation reaction was possibly too slight to be observed in Saito's work. Evidently, there is not universal agreement on the effect of oxygen pressure on the rate of formation of U_3O_7 on UO_2 powders. The bulk of evidence suggests that below a certain threshold ($\sim$ 10 kPa) the rate of oxidation depends strongly on oxygen pressure, whereas there is little, if any, pressure dependence at higher (e.g. atmospheric) pressure.

The oxygen pressure affects not only the rate but also the extent of the oxidation reaction. Anderson et al. [54] found that for oxygen pressures between 0.003 and 70 kPa the end product of UO_2 powder oxidation (130 to 180°C) varied between $UO_{2.21}$ and $> UO_{2.37}$, with a positive correlation between pressure and the degree of oxidation in the final product. They suggested that the pressure dependence of the oxidation reaction may be due to the inhibition of oxidation by a surface skin of well-ordered U_4O_9, which forms during the long reaction times required for low-pressure oxidation. Such a hypothesis is consistent with the findings of Chumachkova et al. [133], who reported that UO_2 powders heated in the range 120 to 200°C with an oxygen pressure of 0.17 kPa oxidized to $UO_{2.34}$ yet retained 'the same fluorite structure as the starting uranium dioxide'.

The effect of oxygen pressure on the rate of formation of U_3O_8 on UO_2 powders has not been extensively studied. Saito [132] oxidized UO_2 powders in the range 175 to 330°C and reported that increased oxygen pressures resulted in shorter induction times and faster formation rates for U_3O_8. Such results are consistent with oxidation experiments performed on sintered UO_2 pellets (Section 2.4.2).

2.4.2. Oxidation of UO_2 sintered pellets

The pressure dependence of the oxidation reaction is somewhat more complicated for sintered pellets than UO_2 powders, because oxidation of pellets proceeds via sigmoidal reaction kinetics (Section 3.3). During the induction period a layer of U_3O_7/U_4O_9 forms on the sample surface, and the nucleation and growth of U_3O_8 is initiated. In the rapid post-induction ('linear') region, the oxidation process is dominated by U_3O_8 nucleation and growth, as well as the rate at which U_3O_8 powder spalls from the sample surface. The effect of pressure on the rate of oxidation must be considered separately for the induction and the post-induction periods.

The effect of oxygen pressure on the rate of oxidation during the U_3O_8 induction period has not been widely studied. Tucker [42] systematically examined the rate of oxidation of advanced gas-cooled reactor (AGR) fuel pellets over a range of temperatures (200 to 500°C) and oxygen partial pressures (0.1 to 27%) in argon. He reported that neither the oxidation rate nor the length of the induction period displays significant pressure dependence. Nakamura et al. [134] reported that the induction time for oxidation of sintered UO_2 pellets at 240°C is longer for mixtures of air (1 or 2%) in argon than for pure air. However, they also stated that the rate of oxidation during the induction period was somewhat faster for a mixture of air (1%) in argon than for pure air, which is difficult to rationalize.

Smith [63] reported that surface oxidation of UO_2 pellets in the range 300 to 400°C results in the formation of a 22-nm-thick layer of U_3O_7 and that the rate (R) of oxidation is proportional to the oxygen partial pressure:

$$R = 5.5 \times 10^{-7} P e^{\{-6440/T\}}, \quad (7)$$

where the rate is given in mol O_2/cm^2 s, P is the oxygen pressure in Torr (1 Torr = 101 326/760 Pa) and T is in Kelvin. Eq. (7) yields an activation energy of 53.6 kJ · mol^{-1}. However, the suggested formation of such a thin, limiting surface layer of U_3O_7 at such high temperatures is inconsistent with more recent studies in which much thicker layers of U_3O_7/U_4O_9 have been observed (see Sections 3.1.2 and 3.2).

All reports concur that the rate of oxidation in the post-induction period increases with increasing oxygen partial pressure. Nakamura et al. [134] found that the linear portion of the sigmoidal reaction curve (Fig. 1) was greater in air than in mixtures of air (1 or 2%) in argon. Similarly, Ohashi et al. [7] reported that the rate of formation of U_3O_8 on UO_2 microspheres increases with oxygen pressure. They also reported that at temperatures below 380°C, the activation energy for the formation of U_3O_8 increases with decreasing pressure. Tucker [42] carefully examined the post-induction reaction rate on AGR pellets in the range 200 to 500°C (0.1 to 27% O_2) and found that the rate (R, mg cm^{-2} h^{-1}) was given by

$$R = KP^{(mT+B)}, \tag{8}$$

where $m = 0.0021$, $B = -0.157$, the temperature is given in °C, P is in atmospheres and K is a proportionality constant.

2.5. Nitrogen oxides (NO_x)

The effect of NO_x on the oxidation of UO_2 may be relevant to fuel storage, because NO_x may be generated in a storage vessel by the radiolysis of air; in the presence of moisture, nitric acid is also formed. The quantities of corrosive materials can be substantial; Wasywich and Frost [95] reported pH values as low as 1.55, with correspondingly high nitrate analyses, for residual water in experiments with used CANDU fuel stored in moist air.

The effect of nitrogen dioxide on the oxidation of UO_2 was studied by Anderson et al. [54], who fitted their kinetic data for the oxidation of unirradiated UO_2 powders to a parabolic rate law. They found that the rate constant, k, for the oxidation of UO_2 is at least twice as great for oxidation in NO_2–O_2 mixtures at ~50 kPa total pressure as compared with reaction in pure oxygen at similar pressures. Also, several authors have shown that in the range 215 to 250°C, NO_2 (1%) in air oxidizes unirradiated UO_2 pellets at a significantly faster rate than oxidation by pure air [19,43,135]. This effect cannot be quantified because there were significant variations in the sample densities used in their work.

In addition to accelerating oxidation, the presence of NO_2 can cause the oxidation reaction to proceed beyond U_3O_8. For example, a non-irradiated UO_2 pellet heated for 600 h at 250°C in NO_2 (1%) in air showed essentially complete conversion to UO_3 [135].

Campbell et al. [43] measured the weight gain for sintered LWR pellets oxidized in static air in the temperature range 200 to 220°C, both with and without an imposed gamma field of 2×10^5 R h^{-1}. Their data were not analyzed quantitatively; however, they observed significantly higher weight gains for those samples oxidized in the gamma field. These findings were attributed to the radiation-induced buildup of NO_x compounds in the static air atmosphere, because samples oxidized in flowing-air atmospheres did not show a comparable effect.

The importance of nitrogen oxides in the dry storage of used fuel will depend on their concentration in the storage atmosphere. Estimates for the amount of NO_x that will be present in a vault vary widely. Spellar et al. [136] found only 5 ppb nitric acid in the ventilated containment system at Wylfa, UK, whereas Johnson et al. [137] found up to 0.25% (vol) NO_2 in air samples surrounding stored LWR fuel. Substantial quantities of nitric acid (pH values as low as 1.55) have been observed in demonstration experiments on the storage of used CANDU fuel in moisture-saturated air at 150°C [95]. It seems likely that NO_x enhancement of the oxidation reaction should be considered for any dry air storage scheme in which the fuel is not ventilated, but quantitative experimental data are limited.

2.6. Radiation

External radiation (gamma or neutron) can affect the oxidation process in two different ways. First, radiolysis of the cover gas can result in the formation of strong oxidants, such as NO_x, H_2O_2 and radical species, which can have a major effect on the rate of oxidation (Section 2.5). Second, radiation introduces lattice defects in the UO_2, which might affect the rate of oxidation by allowing enhanced oxygen diffusion. In the present section, we focus on the latter effect of radiation.

Dominey and co-workers [138,139] reported that the rate of UO_2 powder oxidation (by CO_2) in a reactor neutron flux is approximately the same as the rate of oxidation by O_2 (0.8 to 0.9 kPa) in the absence of radiation fields. The in-reactor temperatures were in the range 60 to 90°C and resulted in the formation of a cubic UO_{2+x} phase with $x < 0.25$ [139]. In contrast, the laboratory experiments (without irradiation) at 66 and 80°C resulted in the formation of tetragonal $UO_{2.33}$ [138]. Presumably, CO_2 would not oxidize UO_2 at a significant rate at such low temperatures, unless the reaction were enhanced by the neutron radiation.

In a more quantifiable test [99] comparatively low levels of neutron irradiation (integrated flux of 10^{20} n m^{-2}) increased the rate of oxidation of UO_2 at 350°C but had no measurable effect at 425 to 500°C. The study included single-crystal UO_2, as well as so-called sintered

annealed and sintered unannealed material. Here, annealing apparently refers to an unspecified heat treatment to increase the grain size of the sintered fuel, to simulate the grain growth that occurs near the centre-line of fuels operating at high power ratings. This typically occurs when centre-line temperatures exceed ~1700°C [16,140].

The influence of irradiation at 350°C was most obvious for monocrystalline material, less apparent for sintered annealed material, and least evident for sintered unannealed UO_2. The rate of weight gain in the region 25 to 75% reaction (to U_3O_8) was measured; irradiation increased this rate by a factor of 4.5 for the monocrystalline material and 2 for the sintered, annealed UO_2, but had no significant effect on the rate of oxidation for the sintered, unannealed UO_2. Even in the presence of radiation, the rate of oxidation still decreased along the series: unannealed > annealed > monocrystalline. The increased rate of oxidation for the irradiated material was attributed to the introduction of defects in this material, especially at low temperatures and in initially defect-free material [99].

Sunder and Miller [77,78] oxidized portions of sintered fuel pellets at 150°C for 2 h in gamma fields equivalent to those associated with used CANDU fuel. They reported that significant quantities of U_3O_8 were present on the surface of such samples. These data may be the result of radiation-enhanced oxidation, but the lack of control samples (i.e. without gamma fields) makes such a comparison difficult. Certainly, the presence of both moisture and gamma fields leads to an increased rate of oxidation [77,78,141].

Used LWR fuel fragments were oxidized in flowing air at 200°C and 230°C [18,135] and it was reported that there are no significant differences in the rate of weight gain between low (10^3 R h^{-1}) and high (1.3×10^5 R h^{-1}) imposed gamma fields. Similar findings were reported for unused LWR fuel pellets [18]. Oxidation tests performed on used LWR fuels in static air at 230°C and an imposed gamma field of 1.5×10^5 R h^{-1} for up to 4000 h displayed a weight gain exceeding 4 wt% [18]. These results were initially thought to be due to the oxidation of the fuel to higher oxides (beyond U_3O_8), but it was subsequently found that the high degree of oxidation in these tests was associated with the presence of fluorine in the static air of the ovens [142]. The fluorine, which originated from radiolysis of fluorocarbon polymer seals, may have also affected the kinetic tests on the influence of radiation on oxidation [18].

The experimental results thus suggest that any effects that external radiation may have on the rate of UO_2 oxidation (other than indirectly by radiolysis of a static cover gas) are likely to be slight. The effect of external radiation on the oxidation process is most likely to be observed for relatively defect-free material such as monocrystalline UO_2 or annealed sintered pellets and less likely observed for highly defective material such as used fuel. Moreover, any effects of radiation on the oxidation process are likely to be significant only at low temperatures, because annealing experiments on low-burnup fuel suggest that oxygen interstitials anneal at around 200 to 300°C, whereas uranium vacancies anneal at 300 to 500°C [61,143–145]. Similarly, high-burnup (25 to 44 MW d/kg U) LWR fuels showed annealing of point defects (perhaps uranium vacancies) in the range 450 to 850°C [146,147].

2.7. Aging in ambient air

The effects of long-term ambient-air storage on the subsequent oxidation of sintered UO_2 pellets has been examined by researchers at PNL [19,43]. They examined a series of LWR-type pellets stored in ambient air for periods up to 2 years and found that air storage results in a dramatic change in the oxidation kinetics. Tests at 180 to 250°C indicated that increased aging leads to slower rates of weight gain, longer powder induction times and the formation of powder at lower O/U ratios. The effects of aging are quite dramatic; for example, air storage for 20 months caused the powder induction time to double (from 2000 to 4000 h) when pellets were subsequently oxidized at 200°C [43]. However, incomplete microstructural analysis of the specimens precluded quantitative interpretation of the results.

The reasons for the effect of aging on oxidation behaviour are not yet fully understood. It has been suggested that aging may cause the formation of a thin coating of highly oxidized material (UO_3 or one of its hydrates), which then acts as a barrier to oxygen diffusion [43,148]. This is consistent with the reported formation of a thin, highly oxidized layer on the surface of UO_2 samples oxidized at low temperatures as observed by infrared [6], XRD [90], Auger [89] and XPS techniques [59]. Specimens of used CANDU fuel retrieved from demonstration storage experiments at 150°C also tend to show higher levels of oxidation when analyzed by XPS, a surface-sensitive technique, as compared with bulk analytical methods [16]. However, a detailed picture of the aging process remains unclear, as does the effect (if any) of aging on used fuel oxidation.

2.8. Physical parameters

2.8.1. Particle size

The rate of the oxidation reaction, and the extent to which oxidation proceeds, are both strongly dependent on the particle size of the UO_2 starting material. Chemisorption and the diffusion-controlled formation of U_3O_7 are both proportional to surface area, and thus it is not surprising that samples with smaller particle sizes (larger surface area) react faster than samples with large particle sizes or sintered pellets. The vast differences in reaction rates are, however, notable. For example, very fine (e.g. 0.05 μm diameter) UO_2 powders react pyrophorically with oxygen at 0°C [54], whereas sintered pellets react only very slowly

with air, e.g. at 250°C an oxide layer 1 μm thick is formed after 24 h [44]. In this section, we focus primarily on the qualitative differences in oxidation behaviour observed for various types and particle sizes of UO_2 samples.

The pyrophoric reaction of finely divided UO_2 with air has received considerable attention because of its obvious practical importance in the fabrication of UO_2 nuclear fuel [2,3,53,54,149]. Anderson et al. [54] showed that UO_2 samples with surface area greater than 8.4 $m^2\ g^{-1}$ are pyrophoric in air at room temperature and Bannister [2] showed that the reaction is driven by the exothermic chemisorption of oxygen. The tendency towards pyrophoric oxidation increases with temperature, oxygen pressure and surface area [53].

In addition to the pyrophoric reaction, powdered UO_2 with a large surface area also displays unusual behaviour in the extent of low-temperature oxidation. Bel and Carteret [150], as well as Lister and Gillies [151], determined limiting compositions for the air oxidation of finely powdered UO_2 at room temperature. Limiting compositions were reported to increase with surface area, to maximum O/M ratios in the range 2.29 to 2.43. Hoekstra et al. [6] oxidized a UO_2 powder that had a high surface area (30 $m^2\ g^{-1}$) and found that it oxidized to the composition $UO_{2.5}$ at 25°C. Cubic UO_{2+x} with x in the range 0.24 to 0.5 is formed when extremely fine UO_2 is oxidized by air at room temperature [85,152–154].

It has been shown [2,55] that the increase in O/M ratio observed over long periods of time, when powdered UO_2 was stored near room temperature [87], can be described in terms of a model that includes chemisorption, sub-surface oxidation and diffusion-controlled bulk oxidation. In essence, the data suggest that a high degree of oxidation can be achieved at low temperatures for finely divided powders because of chemisorption and the formation of a thin (< 2 nm) film of a higher oxide such as hyperstoichiometric UO_{2+x}, UO_3 or a hydrate thereof [6,89,90]. These results are consistent with the effects of air aging described in Section 2.7.

Chemisorption and formation of a thin higher-oxide film can contribute significantly to the bulk composition when the surface area is large. Similar thin oxidized films are important in the oxidative, aqueous dissolution of UO_2 fuel. The extensive work on characterization of these films [60] may also provide insight into air-formed films of the type discussed above.

For powdered UO_2 samples with surface areas below $\sim 5\ m^2\ g^{-1}$, oxygen chemisorption and the formation of a thin film of a higher oxide are less important in the overall oxidation scheme [54]. Instead, such powders display the parabolic kinetic behaviour [155,156] reported for UO_2 by Aronson et al. [1] and Blackburn et al. [4] for the diffusion-controlled oxidation process. In this reaction, the rate of oxygen diffusion is controlled by the thickness of the U_3O_7 oxide layer. The validity of the parabolic kinetic model has been confirmed by Parker et al. [157], who oxidized UO_2 with surface area 0.4 to 0.8 $m^2\ g^{-1}$ in the range 196 to 242°C in oxygen, and by Walker [35], who oxidized powdered UO_2 (2 to 3 $m^2\ g^{-1}$) at 143 to 211°C.

For powders with very large particle size or for sintered pellets, the bulk rate of the diffusion-controlled oxidation to form U_3O_7 becomes relatively slow, because these samples have small surface areas. Thus no significant weight change is observed until temperatures are high enough that U_3O_8 begins to form [28,158]. For example, in contrast to the parabolic kinetics observed for powdered UO_2 samples, Walker [35] reported that sintered pellets and single-crystal electrolytic UO_2 (surface area 0.0405 $m^2\ g^{-1}$) showed sigmoidal reaction kinetics in the range 312 to 352°C. Coarse powders and crushed sintered pellets displayed reaction curves intermediate between parabolic and sigmoidal. A plateau in the weight-gain curves was found at $\sim UO_{2.34}$ for the fine powders, but occurred at lower compositions for the coarser materials. These findings led Walker [35] to suggest that oxidation can proceed directly from UO_2 to U_3O_8, but such a mechanism seems unlikely; rather, the U_3O_7 layer was probably too thin to have an impact on his weight-gain experiments. Similarly, Ohashi et al. [7] found that UO_2 powders displayed a two-stage oxidation process, whereas the thermogravimetric curves displayed only one stage for the oxidation of microspheres. They suggested that the oxidation reaction with microspheres proceeds via UO_2–U_3O_7 and U_3O_7–U_3O_8 interfaces, which progress into the microspheres at approximately the same rate, so that there is a layer of U_3O_7 of constant thickness (1 to 2 μm).

It has been suggested that the kinetics of oxidation of unirradiated fuel pellets are dominated by crack formation associated with the reduction of the lattice parameter resulting from the formation of U_3O_7/U_4O_9. Both intergranular [17,159] and intragranular [57,159] crack formation have been reported and can explain the observed linear portion of the reaction kinetics.

The diffusion-controlled reaction to form U_3O_7 appears to be even less important for single crystals than for sintered pellets. Wang [89] heated a single crystal of UO_2 in air at 145°C for 570 h and did not observe any deviations from cubic symmetry by XRD. The lattice parameter decreased on heating, to a minimum value of 5.4675 Å, which is close to the value reported by Aronson et al. [1] for a composition $UO_{2.1}$, just before appearance of tetragonal products [9]. Subsequent heating of Wang's sample at 270°C for 24 h did not change the crystal symmetry from cubic. Wang's results thus suggest considerably slower

[9] Crystallographic lattice parameters should be interpreted with caution in this system because varying degrees of phase separation ($UO_2/U_3O_7/U_4O_9$) may occur, depending on the thermal history of the specimen. Alekseyev et al. [152] have reported the expression $a_0 = 5.4696 - 0.1495x$ for homogeneous UO_{2+x} powders ($x \leq 0.38$).

oxidation kinetics than reported by Taylor et al. [44], which implies that the rate of oxygen diffusion is much slower in single crystals than in sintered pellets. Wang [89] measured the sputtering profile of his single-crystal sample using Auger analysis and reported that a thin film of UO_3 hydrate is present on the surface and that this film may be responsible for the slow rate of oxygen diffusion. Such analyses should be interpreted with caution because of the ease of reduction of higher oxides to UO_2 during sputtering (Hocking, personal communication, 1996).

The particle-size dependence of the oxidation behaviour of used fuel differs from UO_2 because of the relatively fast grain-boundary diffusion of oxygen that occurs in the former. Thomas and collaborators [12,45,58] oxidized used LWR fuel powders and fragments above 175°C. They found that, in contrast to the situation with unirradiated material, both powders and fragments of used LWR fuel display qualitatively similar oxidation behaviour. With used fuel, an initial rapid rate of weight gain slows to a limiting composition near $UO_{2.4}$. Similar behaviour is observed in samples of different particle size because the rapid rate of oxygen diffusion along grain boundaries leads to simultaneous oxidation of individual grains throughout most of the sample. Thus, the rate of oxidation is related to the grain size rather than the particle size. One cannot, however, assume that oxygen diffusion along the grain boundaries is infinitely fast for all used-fuel specimens. Thomas et al. [13] have shown that air oxidation of used H.B. Robinson LWR fuel at 175°C is non-uniform and can be correlated with the initial location of the sample within the pellet. Near the pellet rim, the rate of oxygen diffusion along grain boundaries is rapid because the fission-gas bubbles are smaller, but more plentiful, than near the centre of the pellet. Such non-uniform diffusion rates may also be responsible for the variability in oxidation rates observed in the early stages of oxidation of a series of used LWR samples [160] at 175 and 195°C.

Einziger and Woodley [92,161,162] have also shown that the oxidation behaviour of used fuel cannot be adequately explained in terms of a model that includes infinitely fast grain-boundary oxidation. Further work [91,93] showed that oxygen diffusion is relatively rapid above 175°C so that the rate of oxidation is independent of particle size at these temperatures. However, at lower temperatures the particle size of used-fuel samples becomes important. Einziger and Buchanan [91] showed that at 130°C the rate of oxidation is approximately proportional to the reciprocal of the particle radius, as would be expected for a surface-area controlled reaction. Clearly, an understanding of the temperature dependence of the rate of oxygen diffusion along grain boundaries in used fuel would assist model development.

The second stage of oxidation of UO_2 proceeds via a nucleation-and-growth mechanism and, therefore, it too is likely sensitive to the particle size of the starting material. For sintered pellets, the rate of U_3O_8 formation appears to vary with surface roughness [10,57], which is presumably related to the number of nucleation sites. Similarly, one expects the concentration of nucleation sites, and thus the tendency for U_3O_8 formation, to increase with surface area for powdered samples. Araoz [163] and Kolar et al. [158] have shown that samples with small particle sizes indeed oxidize to U_3O_8 at lower temperatures than those with larger particle sizes. Others have reported on the particle-size dependence of the oxidation curves [164,165], but it is difficult to determine the exact role which particle size plays in U_3O_8 formation.

2.8.2. Grain size

The effect of grain size on the rate of oxidation of sintered UO_2 pellets has recently attracted attention because of reported differences in oxidation behaviour between unirradiated CANDU, AGR and LWR pellets [43,166]. Tests at PNL showed that there is a negative correlation between grain size and the initial (i.e. pre-powdering) oxidation rate of whole pellets in air at 200° and 220°C [43,167]. This is consistent with more rapid oxygen diffusion along grain boundaries than into UO_2 grains, so that oxidation proceeds initially along the grain boundaries and is followed by intragranular oxidation. However, it should be noted that in the PNL study the largest grains were found in the AGR pellets, which also had the highest density; thus, it is not entirely clear that sample density (Section 2.8.3) did not have an effect on the grain-size test. Indeed, it is generally difficult to separate the effects of grain size and sintered density.

Wood and Bannister [168] oxidized a series of sintered pellets in the range 275 to 450°C and noted a positive correlation between induction time and sample grain-size/density. However, as with the pre-induction weight-gain tests, described above, there was a correlation between sample density and grain size, so it is not clear whether the observed correlation is due to grain size or sample density.

The effect of grain size on the maximum rate of oxidation (in the sigmoidal reaction curves) was also studied by Wood and Bannister [168]. They found that the reaction rate increases with decreasing grain size, but only for those samples with grain sizes below ~ 5 μm. Samples with grain sizes larger that 5 μm (up to 24 μm) and single crystals all oxidized at the same rate. Wood and Bannister [168] attributed the insensitivity of oxidation rate to grain size (for the larger grain sizes) as an indication that cracking, which allows ready ingress of oxygen into the sample, controls the oxidation rate in these materials.

The effect of grain size on the oxidation of used fuel was examined by Thomas et al. [45], who oxidized a series of LWR used-fuel fragments and coarse powders at 175 and 195°C and reported similar behaviour regardless of grain size. Their findings are somewhat surprising, because the very rapid rate of grain-boundary oxidation in used fuel leads one to expect the same dependence on grain size

as that of particle size reported for UO_2 powders (i.e. the oxidation rate should be proportional to $1/r$, where r is the mean particle radius). However, the range of grain sizes used in their study was quite small (from 7–15 to 20–30 μm) so the effect of grain size may have been obscured by sample-to-sample variations in oxidation rate.

One might expect that the effect of grain size would be most obvious in experiments with single crystals, which can be considered equivalent to sintered material having only a single grain. In fact, oxidation experiments on small single crystals have shown qualitatively similar behaviour to sintered pellets; that is, weight-gain experiments display the sigmoidal growth kinetics for U_3O_8 formation, at similar temperatures to which U_3O_8 is formed on powdered samples [35,169]. Similarly, the growth of the thin surface layer of U_3O_7 on single-crystal UO_2 is expected to be similar to that observed on sintered pellets [44]. However, experiments on single crystals have given varied results.

Wang [89] observed very slow rates of oxidation for a single-crystal slice [111 orientation] of UO_2. For example, Auger spectroscopy indicated that a sample oxidized for 24 h in air at 285°C had oxygen penetration only 2 nm below the sample surface, which is far less than expected from air-oxidation rates of sintered polycrystalline UO_2 [44]. As noted in the preceding section, however, the sputtering technique used to obtain the depth estimate may not be reliable, because higher oxides of uranium tend to revert to UO_2 under ion bombardment (Hocking, personal communication, 1996). In contrast to Wang's results, Allen et al. [170,171] found that single-crystal slices cut parallel to the [111], [110] or [100] crystallographic planes oxidized to U_3O_7 faster than polycrystalline material. They suggested that these results were due to the inability of polycrystalline UO_2 to accommodate lattice strains (associated with the molar volume changes concomitant with the oxidation process) across grain boundaries.

Regardless of the details of U_3O_7 formation on single-crystal UO_2, it is certain that the second stage of oxidation of this material (to U_3O_8) proceeds by a nucleation and growth mechanism, as expected. Sigmoidal reaction kinetics are observed for the formation of U_3O_8 on single crystals [35], similar to the situation with sintered pellets; thus the spalling process is similar for these types of materials. Wood and Bannister [168] showed that the rate of formation of U_3O_8 on single crystals of UO_2 is similar to that on sintered materials with grain sizes > 5 μm, suggesting that the cracking and spalling processes, which are rate limiting for sintered materials, also occur in single crystals.

2.8.3. Pellet density

Increased pellet density has been found to correlate with a decreased rate of oxidation during the induction period for unirradiated UO_2 pellets, provided the sample is below 95% theoretical density (TD [10]) [66,134]. Similarly, Campbell et al. [43] noted that high-density pellets displayed a lower weight gain than low-density pellets when a series of samples ranging from 94 to 95.5% TD were oxidized at 220°C. The increased reactivity for low-density material has been attributed to increased open porosity [134,172].

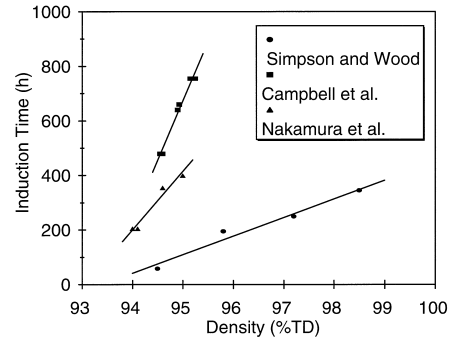

Fig. 4. Induction time (t_i) as a function of sample density for the oxidation of unirradiated UO_2 in air. The oxidation conditions were 250°C in 'ordinary laboratory air' for the data by Simpson and Wood [9], 240°C in 'air' for Nakamura et al. [134] and 220°C in air with a dew point of −35°C for Campbell et al. [43].

Above ~95% TD the density dependence of oxidation behaviour is less apparent than at lower values; any correlation between density and oxidation rate must be slight. Simpson and Wood [9] studied the oxidation of unirradiated AGR pellets in air at 250°C. Pellets with densities in the range 10.36 to 10.81 g cm^{-3} (94.5 to 98.6% TD) all showed essentially the same rate of weight gain during the induction period. Such results are consistent with the work of Nakamura et al. [134], who reported that the oxidation rate during the induction period is not very sensitive to sample density for samples whose density is above ~95% TD.

The slope of the linear portion of the sigmoidal oxidation curve displays a density dependence similar to that observed in the induction period. Below ~95% TD the rate of oxidation increases significantly with decreasing density [134,168]. In contrast, Wood and Bannister [168] reported that the rate of oxidation does not depend on density for those samples that have densities greater than 10.65 g cm^{-3} (97.2% TD; grain sizes greater than ~5 μm). Presumably, the oxidation behaviour in the post-induction period is related to improved access of oxygen to the interior of the sample in low-density samples. Samples that are > 95% TD tend to have very little open porosity, and thus tend to oxidize at the same rate.

The rate of oxidation of high-density samples is similar to rates obtained for single crystals of UO_2 [168]. It was

[10] The theoretical density of natural UO_2 is 10.96 g cm^{-3}.

thus suggested that cracking patterns that occur in partially oxidized UO_2 grains are rate limiting; that is, when the oxidized layer reaches a thickness of about 2 μm, stress-induced cracking provides a pathway for oxygen access to the underlying UO_2.

A positive correlation between the induction time (t_i) and the sample density was first reported by Simpson and Wood [9]. Since then the relationship between t_i and density has been confirmed [19,43,134,167,168] as shown in Fig. 4. It should be noted, however, that in many cases there was a correlation between density and particle size [43,167,168] and that the effects of density and particle size are difficult to separate.

In summary, it is certain that the rate of oxidation (both before and after the induction period) decreases with increasing sample density. The low reactivity for high-density UO_2 is possibly related to the low open porosity in such samples. Below ~95% TD, there is a clear relationship between density and reactivity, whereas at higher densities the relationship is less obvious. Similarly, it is certain that higher densities are associated with longer induction times. For both rates and induction times, however, it is difficult to make firm conclusions as to whether the observed behaviour is associated with sample density or systematic differences in fuel characteristics (e.g. porosity, grain-boundary diffusion rates, grain size, etc.) resulting from the fabrication process.

2.8.4. Orientation effects

2.8.4.1. Formation of U_3O_7/U_4O_9. Taylor et al. [44] used XRD to study the formation of U_3O_7 on sintered UO_2 disks and found that oxidation proceeds initially via the formation of a uniform thin layer of U_3O_7. Their data gave evidence of preferred-orientation effects, that is, generally the intensity of one member of each U_3O_7 multiplet was enhanced relative to the others. Thus, for example, UO_2 grains with the [100] plane parallel to the sample surface preferentially oxidized to U_3O_7 with [100] rather than [001] parallel to the surface, and hence the $h00$ diffraction peaks are strongly enhanced relative to $00l$. Taylor et al. [44] concluded that the preferred orientation effects were probably related to the minimization of stress in the oxidized surface layer.

Allen et al. [170,171] reported that the rate of U_3O_7 formation on oriented slices of UO_2 followed the order [111] > [110] > [100] > [polycrystalline] when oxidized in 0.13 kPa O_2 at 225°C. They interpreted this in terms of the relative ease with which oxygen interstitials at the U_3O_7/UO_2 interface can cluster into the ordered U_3O_7 structure. The structure they previously proposed, however, has been shown to be incorrect [24,173]. Teixeira and Imakuma [11] also published evidence for anisotropic oxidation of UO_2. They reported that the activation energy for the formation of U_4O_9 on UO_2 was significantly lower for oxidation in the [100] direction, based on measurement of the [200] peak intensities (90 kJ mol^{-1}) than in the [311] direction (117 kJ mol^{-1}). However, their conclusions have been questioned by McEachern and Taylor [174], who re-analyzed the data using a thin-film model and found no significant differences between the activation energy for oxidation in the two crystallographic directions.

The studies by Allen et al. [170,171] and Teixeira and Imakuma [11] suggest that the rate of formation of U_3O_7/U_4O_9 on crystalline UO_2 differs for the various crystallographic directions. In contrast, the results obtained by Taylor et al. [44] and McEachern and Taylor [174] suggest that the formation of U_3O_7/U_4O_9 on sintered UO_2 pellets occurs initially by the formation of a uniform thin layer with only minor preferred-orientation effects. We thus conclude that any variations in the rate of formation of U_3O_7/U_4O_9 in the various crystallographic directions are slight. This conclusion is supported by the evidence from SEM studies of uniformly thick layers of U_4O_{9+y} around individual grains in used LWR and CANDU fuel [12,16].

2.8.4.2. Formation of U_3O_8. There is strong evidence that the rate of formation of U_3O_8 on single-crystal UO_2 is dependent on crystallographic orientation. Allen et al. [64,175] oxidized single-crystal specimens with polished surfaces cut parallel to the [111], [110] or [100] faces. For comparison, they also oxidized polycrystalline UO_2 disks. The oxidation reaction in 0.13 kPa O_2 at 300°C was studied by XPS, SEM and XRD and it was found that the reactivity follows the sequence [111] > [110] > [100] > [polycrystalline].

Allen et al. [64,175] proposed that the rapid rate of oxidation in the UO_2 [111] direction, and the concomitant formation of U_3O_8 in the [001] direction, are the result of an epitaxial relationship between these crystallographic directions. They suggested that ordered interstitial oxygen clusters in the fluorite structure may be related to the $(UO_2)O_5$ pentagonal bipyramids in the U_3O_8 structure and that the changes in the oxygen lattice are the driving force for the formation of U_3O_8. In support of this theory they showed that there is a close correspondence between the uranium ion locations in the UO_2 [111] planes and their locations in the U_3O_8 [001] plane; conversion of UO_2 to U_3O_8 involves a shear-displacement of the uranium sublattice from an ABCABC… sequence to AAA… stacking [176]. Moreover, the increase in the interplanar spacings ($d_{111}(UO_2) = 0.3156$ nm; $d_{001}(U_3O_8) = 0.4147$ nm) between the UO_2 [111] plane and the U_3O_8 [001] plane accounts for 88% of the molar volume increase associated with the reaction. They thus concluded that the rapid rate of oxidation of UO_2 sliced parallel to the [111] plane is due to the relative ease with which the lattice can expand in the direction normal to this surface. In contrast, for the [110] and [100] planes and for the polycrystalline material, lattice expansion is not readily accommodated.

The findings of Allen et al. [64,175] are supported by Taylor et al., who reported that the XRD peaks associated with the [001] planes of U_3O_8 were disproportionately intense when polished, sintered UO_2 disks were oxidized in air below 250°C [10] or in aerated water at 225°C [72].

3. Oxidation mechanism and activation energy

3.1. Reaction mechanism

3.1.1. Oxidation of UO_2 powders

It is generally accepted that the first stage of oxidation is the incorporation of small quantities of oxygen into the fluorite-type lattice to form hyperstoichiometric UO_{2+x}:

$$UO_2 \rightarrow UO_{2+x}. \tag{9}$$

The proposed reaction mechanism in which oxidation to U_3O_7/U_4O_9 proceeds into UO_2 grains along a concentration gradient of oxygen can be dismissed (Section 3.2), however, there appears to be a small, but finite solubility for oxygen in the UO_2, which is a function of temperature.

There remains some uncertainty in the exact limits of non-stoichiometry in UO_{2+x}. Smith et al. [49] indicated that the limit of non-stoichiometry is $UO_{2.04}$–$UO_{2.07}$ at ambient temperature, $\sim UO_{2.15}$ at 400 to 600°C and $UO_{2.25}$ at 1100°C, but it seems likely that these limits are too high. Blackburn et al. [4] studied the lattice parameter of UO_2 for the oxidation of sintered pellets (0.032 $m^2\ g^{-1}$) and powders (0.57 $m^2\ g^{-1}$) in the range 100 to 280°C and reported that the solubility of oxygen in UO_2 is ~ 0.01 or less, that is, the upper boundary of the UO_{2+x} phase field occurs at $x \leq 0.01$ and further addition of oxygen yields U_3O_7 or U_4O_9, rather than a more oxygen-rich UO_{2+x} phase. Blackburn et al. [4] noted that this conclusion was consistent with the phase diagram proposed by Grønvold [177]. Similarly, Hoekstra et al. [6] reported that the maximum value of x is < 0.03 for the oxidation of UO_2 powders (0.05 to 0.5 $m^2\ g^{-1}$) in the range 120 to 250°C. Schaner [178] carefully examined the UO_2–U_4O_9 phase diagram by metallographic techniques and reported very low limits of non-stoichiometry; for example, the maximum value of x was reported as < 0.01 at 350°C. The source of confusion in determining the maximum degree of hyperstoichiometry is likely the formation of a highly oxidized surface layer that readily forms on the surface of UO_2 (Section 2.8.1).

It is generally accepted that the basic reaction scheme for the oxidation of UO_2 powders, beyond UO_{2+x} involves U_3O_7 formation [6]:

$$UO_{2+x} \begin{cases} \nearrow\ \alpha\text{-}U_3O_7\ (a = 0.546\ \text{nm},\ c = 0.540\ \text{nm},\ c/a = 0.989) \\ \searrow\ \beta\text{-}U_3O_7\ (c/a = 1.031) \end{cases} \tag{10}$$

The unit-cell parameters given in Eq. (10) represent only the overall distortion of the fluorite-type lattice and they cannot adequately describe ordered U_3O_7 structures. Indeed, recent TEM studies (Thomas and Taylor, unpublished observations) have shown that β-U_3O_7 has a superlattice structure with $a(U_3O_7) = \sqrt{5}\,a(UO_2)$ and $c(U_3O_7) = 3a(UO_2)$.

The product formed in the early stages of the oxidation reaction is α-U_3O_7. In general, oxidation proceeds from UO_2 to α-U_3O_7 and then on to β-U_3O_7; however, it appears that at low enough temperatures the oxidation process does not reach the β product. Conversely, at high enough temperatures (150 to 265°C) β-U_3O_7 can form directly from UO_2 [179]. Thus α-U_3O_7 was the major product when UO_2 powders were oxidized at 135°C [179], 120 to 160°C [6], 200°C [132], or 120 to 175°C [180,181], whereas β-U_3O_7 was the major product of air oxidation of UO_2 powders at 225°C [179], 160 to 250°C [6], 210 to 299°C [35], 340°C [132], 225 to 250°C [9] or 200 to 250°C [182]. Retention of α-U_3O_7 also appears to be favoured by large sample surface areas [6].

As discussed in detail in Section 3.2, the measurement by XRD of crystallographic data of the intermediate products was used to determine the mechanism behind the oxidation kinetics. The careful analysis by Hoekstra et al. [6] of XRD patterns gave strong support to the discrete-layer mechanism and suggested that earlier work, which had shown the smooth progression of c/a ratios (from 1.00 to 1.03) over the course of oxidation, arises from the poor resolution of conventional film techniques [1,128].

Reports of intermediate phases with c/a ratios between those of α-U_3O_7 (0.989) and β-U_3O_7 (1.03) persist. Kuz'micheva et al. [183] reported that the non-isothermal oxidation of UO_2 powders in air in the range 100 to 150°C results in the formation of a product with a c/a ratio of 1.01 to 1.02. Similarly, Walker [35] oxidized UO_2 powder and found that products with $c/a = 1.006$ and 1.017 were formed at 135°C and 182°C, respectively. Saito [132] reported that oxidation at 240°C results in the formation of material with $c/a = 1.020$ (which he labelled β'-U_3O_7), similar to the $UO_{2.3}$ phase reported by Hoekstra et al. [6] for the oxidation of U_4O_9. Recent studies [7] have also shown that deconvolution of the XRD peaks suggests that β'-U_3O_7 is formed after α-U_3O_7. Blackburn et al. [4] observed c/a ratios between 1.01 and 1.03 during the oxidation of UO_2 powders at 150°C and 200°C. They attributed these results to the distortion of the U_3O_7 lattice by the underlying UO_2, because deviations from $c/a = 1.03$ were only found for those samples that had small quantities of U_3O_7. In conclusion, it is not possible, based on present evidence, to decide with certainty whether the reported phase with $c/a \sim 1.015$ is genuine, the result of a strained U_3O_7 lattice, or an artifact of the convolution of peaks associated with a mixture of UO_2, α-U_3O_7 and β-U_3O_7. The situation is further complicated by reports of additional tetragonal or lower-symmetry phases with com-

positions between $UO_{2.3}$ and $UO_{2.4}$ [49]; detailed discussion of these phases is beyond the scope of the current review.

In addition to the confusion over the possible existence of a phase with $c/a \sim 1.015$, there have also been reports of U_4O_9 as an intermediate in the oxidation of UO_2 disks and powder [131,184,185]. Recent TEM evidence suggests that β-U_4O_9 microdomains may exist within predominantly β-U_3O_7 layers on air-oxidized UO_2 (Thomas, personal communication, 1995). Nevertheless, although low oxygen pressures favour formation of U_4O_9 (Section 2.4), it is unlikely that it ever occurs as a major product at ambient oxygen pressures.

Samples heated above ~ 200°C will nucleate U_3O_8 and the oxidation reaction proceeds further [6]:

$$\beta - U_3O_7 \rightarrow U_3O_8. \quad (11)$$

It has been reported [6,132] that U_3O_8 forms only on samples that contained β-U_3O_7. It has therefore been proposed that U_3O_8 nucleates at specific sites on the β-U_3O_7 structure [6]. Such a hypothesis seems reasonable, but there is as yet no conclusive evidence to support it. Other reported intermediates in the formation of U_3O_8 include U_8O_{21} [183], $UO_{2.6-x}$ [131] and tetragonal $UO_{2.56}$, on which the U_3O_8 nucleates [186], but the role of such phases remains unproven. Merging Eqs. (9) and (10) and (11) yields the simplified overall reaction mechanism for the oxidation of UO_2 powders:

$$\begin{array}{ccccc} UO_2 & \rightarrow & UO_{2+x} & \rightarrow & \alpha\text{-}U_3O_7 \\ & \searrow & & \downarrow & \\ & & & \beta\text{-}U_3O_7 & \rightarrow \ U_3O_8 \end{array} \quad (12)$$

3.1.2. Oxidation of sintered pellets

The oxidation behaviour of sintered pellets is similar in many ways to the oxidation of powders. At moderate temperatures (230 to 360°C) a layer of material resembling β-U_3O_7 ($c/a = 1.03$) is formed on the surface of the sample and grows inward following diffusion-controlled kinetics [4,35,44]. Later, U_3O_8 nucleates and grows on the U_3O_7 [10]. At temperatures below ~ 150°C, where α-U_3O_7 is the expected product of UO_2 powder oxidation, the rate of oxidation of UO_2 disks is very slow [44] and has not been intensively studied. The formation of α-U_3O_7 with $c/a < 1.00$ under such conditions has not yet been reported.

Tempest et al. [57] oxidized AGR fuel disks at 230°C and reported the formation of a tetragonal phase with $c/a = 1.015$. They noted that this material resembles the high pressure γ-U_3O_7 phase and suggested that such a material may be formed because of stresses induced as a result of the volume change associated with oxidation. Such stresses may result in the formation of material with low c/a (1.015) because reaction occurs fastest for material with c parallel to the sample surface, whereas expansion of the grains in the c direction is impeded because of the neighbouring grains. Preferred orientation effects for the formation of U_3O_7 are discussed further in Section 2.8.4.

3.1.3. Oxidation of used fuel

The oxidation mechanism for used fuel differs from that of UO_2 in one major aspect. Whereas oxidation of UO_2 proceeds by way of the tetragonal α-U_3O_7 and β-U_3O_7 phases, used LWR fuel typically oxidizes to a cubic phase that resembles U_4O_9 but has a composition near $UO_{2.4}$ [45]. The behaviour of used CANDU fuel appears to be intermediate between that of UO_2 and used LWR fuel [16]. The differences in oxidation behaviour between unirradiated UO_2 and used fuel have been attributed to the high concentrations of fission products found in the latter, as discussed in Section 2.3.

Recent studies [45] have shown that the U_4O_9-type phase formed by the low-temperature oxidation of used LWR fuel does not have the highly ordered superstructure [25] associated with β-U_4O_{9-y} (which is the stable form of U_4O_9 between 80 and 600°C). Instead, it displays diffuse scattering similar to the high-temperature γ-U_4O_9 phase. Thomas et al. [45] concluded that the diffuse scattering pattern was probably observed because used fuel contains microdomains of ordered material, but it lacks long-range structural order. The lack of long-range order is likely due to a combination of radiation damage and disruption of the U_4O_9 superlattice by fission products.

3.2. Kinetics for the formation of U_3O_7/U_4O_9

Here we discuss the kinetics of the reaction

$$UO_2 \rightarrow U_3O_7/U_4O_9. \quad (13)$$

As discussed in Section 2.3, U_3O_7 is the product of low-temperature oxidation of unirradiated fuel or UO_2 doped with only low concentrations of impurities, whereas U_4O_{9+y} is the product of oxidation of used fuel or UO_2 with high concentrations of impurities [43,45]. We assume herein that the mechanism for the formation of U_3O_7 is essentially the same as that of U_4O_{9+y} because these two phases have closely related structures and because parabolic kinetics are observed in either case.

There is general agreement that the parabolic kinetics for formation of U_3O_7/U_4O_9 on UO_2 powders indicates a diffusion-controlled mechanism [1,6,11,54,128,132,187–189]. Two different mechanisms, however, are consistent with the diffusion-controlled kinetics; we consider, for illustration, oxidation of UO_2 spheres of radius, r. First is the concentration-gradient mechanism, in which it is assumed that there is adequate solubility of oxygen in UO_2 to form a solid solution, UO_{2+x}, with a concentration gradient inside the particle, that is, with the O:U ratio decreasing radially from the surface to the interior. The

material is then converted to U_3O_7/U_4O_9 when enough oxygen has been incorporated into the lattice so that its composition is in the range $UO_{2.25}$ to $UO_{2.34}$. According to this mechanism, the fraction of the material (C) oxidized at time (t) can be approximated by the expression [1,190]

$$C = 1 - \frac{6}{\pi^2}\sum_{n=1}^{\infty}\left(\frac{1}{n^2}\right)\exp\left(-\frac{\pi^2 n^2 D^{O} t}{r^2}\right), \tag{14}$$

where D^{O} is the diffusion coefficient of oxygen in UO_2.

The values of the chemical diffusion coefficient, as determined by Aronson et al. [1] yield kinetic data typical of those for U_3O_7 formation [62]. Moreover, the diffusion coefficients reported by Aronson et al. [1] are in reasonable agreement with high-temperature data (see Section 2.1) considering the uncertainty in the experimental data and the dependence of the rate of oxygen diffusion on the degree of non-stoichiometry.

The second, discrete-layer mechanism has also been used to describe the formation of U_3O_7/U_4O_9 on UO_2. According to this model, oxidation proceeds by the formation of a discrete surface layer of U_3O_7/U_4O_9, which thickens with time. The rate of reaction in the discrete-layer model is limited by the rate of diffusion of oxygen through the U_3O_7/U_4O_9 layer. The thickness, X, of the product layer is given by Eq. (15), in accordance with Refs. [4,33,34,191]:

$$X = ra\left[1 - (1 - C)^{1/3}\right] = \sqrt{kt}\,, \tag{15}$$

where a is the ratio of the molar volume of U_3O_7/U_4O_9 to that of UO_2, C is the fraction of UO_2 converted to U_3O_7/U_4O_9, and k is the rate constant.

Parabolic rate constants (k) obtained from Eq. (15) can be compared with the chemical diffusion coefficients (D^{O}) for oxygen in UO_2. The bulk of experimental evidence [4,6,178] suggests that the solubility of oxygen in UO_{2+x} is very low in the temperature range of interest ($< 400°C$). If one thus assumes that the solubility of oxygen in UO_{2+x} is negligible, then the parabolic rate constant (k, $m^2\ s^{-1}$) is given by [192]

$$k = 2V_{MO} D^{O} \Delta C, \tag{16}$$

where V_{MO} is the volume of the oxide formed per mole of atomic oxygen combined ($m^3\ mol^{-1}$) and D^{O} is the chemical diffusion coefficient ($m^2\ s^{-1}$). The parameter ΔC (mol m^{-3}) describes the concentration gradient of 'free' oxygen (i.e. over that of UO_2) across the U_3O_7 layer. At the air/U_3O_7 interface we assume that the oxide is pure U_3O_7 so that the concentration of free oxygen is 1 mol (O)/mol U_3O_7, i.e.

$$C = \frac{1}{V_{MO}}. \tag{17}$$

In contrast, the U_3O_7 at the U_3O_7/UO_2 interface is likely to be slightly depleted in oxygen. The change in the concentration of oxygen across the U_3O_7 layer (i.e. ΔC) is difficult to estimate; it is probably quite small because discrete oxide layers can be observed directly by SEM during the course of oxidation reactions [12,193]. If we assume that there is 1% less 'free' oxygen at the UO_2/U_3O_7 interface than at the air/U_3O_7 interface, then

$$\Delta C = \frac{0.01}{V_{MO}} \tag{18}$$

so that

$$k = 2V_{MO} D^{O}\left(\frac{0.01}{V_{MO}}\right) \tag{19}$$

or

$$D^{O} = 50k. \tag{20}$$

Experimental values of k were recently compiled and evaluated by McEachern [62], who reported that the parabolic rate constant is described by the expression

$$\ln(k) = -\frac{95.7\ \text{kJ mol}^{-1}}{R}\frac{1}{T} - 17.33. \tag{21}$$

Eq. (21) gives a value of $3.0 \times 10^{-13}\ m^2\ s^{-1}$ for k at 1000 K which corresponds to a value of D^{O} of $1.5 \times 10^{-11}\ m^2\ s^{-1}$, which is identical with the value put forward by Matzke [194] for the chemical diffusion of oxygen in UO_2 at 1000 K. Similarly, the value of 95.7 kJ mol^{-1} for the activation energy for the parabolic rate constant (Eq. (21)) is in excellent agreement with the suggested value of 96 ± 8 kJ mol^{-1} for the activation enthalpy of the oxygen chemical diffusion coefficient in UO_2 [194].

The two different diffusion-controlled mechanisms represented by Eqs. (14) and (15) yield nearly identical reaction curves [11] [1,4,128,162]. Two different schools of thought thus evolved, and various arguments were presented to support one or the other view.

Aronson et al. [1] recognized that the concentration-gradient mechanism was perhaps over-simplified but concluded that it was valid because they did not observe a tetragonal phase by XRD until the reaction had proceeded to the overall composition $UO_{2.16}$. However, the UO_2 starting material they used was a fine powder (0.5 μm particle radius, as determined by surface area measurement). If the product of oxidation were actually a layer of U_3O_7 on the surface of the UO_2 particles, then the composition $UO_{2.16}$ would correspond to the formation of an oxide layer ~ 0.1 μm thick. Measurement of the XRD pattern of a 0.1-μm-thick oxide layer on the surface of 0.5 μm UO_2 particles is likely to display line-broadening or

[11] In the range $0 < C < 1$. For times exceeding $C = 1$ (i.e. complete reaction) Eq. (15) does not yield physically meaningful results.

lattice strain effects, which obscure tetragonal splitting. Thus, the arguments presented by Aronson et al. [1] in favour of the concentration-gradient model may not be valid.

Anderson [195] as well as Anderson et al. [54] reported that XRD line profiles are consistent with the concentration-gradient mechanism, although they recognized that under some temperatures and pressures the formation of a surface skin of an oxidized product may inhibit further oxidation.

Pério [180,188,189] reported that UO_2 oxidation proceeds by the formation of a skin of tetragonal U_3O_7, in agreement with the discrete-layer mechanism. Blackburn et al. [4] also concluded that the discrete-layer mechanism is operative, because they observed tetragonal U_3O_7 by XRD at overall compositions as low as $UO_{2.06}$ when they oxidized UO_2 pellets. Furthermore, they suggested that earlier workers [54,128] supported the concentration gradient method because the small particle-size material used in those studies had resulted in an overall high degree of oxidation before the U_3O_7 phase could be detected by XRD. Hoekstra et al. [6] carefully examined the products of the oxidation of coarse UO_2 powders using a diffractometer and found evidence for the formation of a tetragonal phase very early in the oxidation reaction. They concluded that the slight deviations from cubic symmetry were not observed in earlier works [54,128] because of the relatively poor sensitivity of XRD film techniques. Hoekstra et al. [6] also reported that the lattice constant for the UO_{2+x} phase remains nearly constant over the course of oxidation, indicating that there is very little solid solution of oxygen in UO_{2+x} in the range 100 to 300°C, consistent with the findings of Grønvold [177] and Schaner [178]. Saito [132] oxidized UO_2 powders in a mixture of 1:4 oxygen:argon at 175 to 275°C and reported that the oxidation kinetics could be fitted to Eq. (15). Moreover, based on detailed XRD analysis of powders oxidized to varying degrees, he suggested that oxidation proceeds by the discrete-layer mechanism, with the first oxidation product, α-U_3O_7 ($c/a = 0.989$), formed at an early stage of the reaction. Teixeira and Imakuma [11] studied the surface oxidation of UO_2 disks by in situ high-temperature XRD. They reported that the oxidation data could be fitted reasonably well to Eq. (15) even though this equation was originally derived for UO_2 spheres rather than disks. In a similar test, Taylor et al. [44] studied the angular dependence of the intensities of the U_3O_7 and UO_2 XRD peaks for CANDU fuel pellets oxidized in the temperature range 225 to 275°C. They found that U_3O_7 progresses initially as a uniformly thick layer; however, in the latter stages of reaction the XRD patterns correspond more closely to a homogeneous mixture. The authors concluded that deviations from a uniformly thick U_3O_7 layer were probably due to the convolution of this layer into an oxidation front that results from the relatively rapid rate of oxygen diffusion along grain boundaries [44].

The bulk of the evidence now supports the discrete-layer mechanism. The detection of U_3O_7 on the surface of sintered pellets or powder that has a large particle size [4,6] suggests that earlier workers [1,54,128,195] did not observe the tetragonal phase in the early stages of oxidation because the deviations from cubic symmetry are only slight and because the formation of a thin surface layer of highly oxidized material results in high weight gains at an early stage of the reaction for fine powders.

Recent work using backscattered-electron SEM imaging [12,193] has allowed the direct observation of the formation of U_4O_{9+y} in used fuel. Thomas and collaborators [12,45] have thus shown clearly that dry-air oxidation at 175 to 195°C proceeds rapidly along the grain boundaries and is followed by intragranular oxidation, which proceeds by the formation of a discrete layer of U_4O_{9+y}. In some cases, they have also observed the presence of an oxidation front in used fuel [13], similar to those observed in CANDU fuel by Wasywich et al. [16]. However, the formation of a discrete product layer, as opposed to an extended composition gradient, was consistently observed. Grain-boundary oxidation is much more limited, or not observed at all, in unirradiated, sintered UO_2 specimens [13,71].

In contrast to the case of UO_2 powders and used fuel, oxidation of unirradiated sintered UO_2 pellets does not, in general, display parabolic kinetics [12,44,57,63]. It seems likely that the initial formation of U_3O_7 on the surface of sintered pellets proceeds as a uniform layer, which thickens according to parabolic kinetics [4]. The form of the kinetic expression changes, however, as the U_3O_7 layer takes on the shape of a convoluted 'oxidation front' because intragranular oxidation proceeds more slowly than oxidation along grain boundaries [44]. It should be noted that this phenomenon is much less prevalent in unirradiated LWR fuel, as compared with CANDU fuel [13,58,71].

Intergranular cracking, caused by the small reduction in molar volume associated with the first stage of oxidation (to U_3O_7/U_4O_9) and possibly also intragranular microcracking at U_3O_7 domain boundaries, provide rapid access of oxygen to the interior of the fuel, close to the reaction front. This may dominate the kinetic expression by controlling the rate of ingress of oxygen to the sample [12,57]; diffusion-controlled oxygen transport through a limiting layer of uncracked product at the reaction front could then lead to linear oxidation kinetics.

3.3. Kinetics for the formation of U_3O_8

In contrast to the ambiguity with the mechanism for the formation of U_3O_7/U_4O_9, there is widespread agreement that a sigmoidal kinetic model describes the formation of U_3O_8 [5,9,18,28,35–37,134,168]. The sigmoidal reaction kinetics observed for the formation of U_3O_8 on UO_2 powders was interpreted by Aronson et al. [1] in terms of a nucleation-and-growth reaction mechanism, using the

mathematical model first derived by Johnson and Mehl [38,39]. In this model, the fraction, α, of the material converted to U_3O_8 is given by the sigmoidal-type expression

$$\alpha = 1 - e^{-(\pi/3)N_v G^3 t^4}, \quad (22)$$

where N_v is the rate of nucleation, G is the isotropic rate of growth of U_3O_8 nuclei and t is time. The kinetics for the formation of U_3O_8 have also been described in terms of the more general (but less instructive) Avrami–Erofeev equation [40,41,196]

$$-\ln(1-\alpha) = (kt)^n, \quad (23)$$

where k and n are empirically determined constants.

Analysis of the U_3O_8-formation kinetics has recently been expanded and improved by McEachern et al. [197], who developed a two-dimensional model for the nucleation-and-growth of U_3O_8 on the surface of a sintered UO_2 disk. They found that U_3O_8-formation kinetic data could be accurately modelled as simultaneous nucleation and growth processes, with the expression

$$\alpha(t) = 1 - \exp\left\{ -\frac{\pi\kappa t^3}{3} + \frac{\pi^2\kappa^2 t^6}{180} - \frac{11\pi^3\kappa^3 t^9}{45\,360} + \frac{5\pi^4\kappa^4 t^{12}}{399\,168} \right\}, \quad (24)$$

where K is a composite rate constant given by

$$\kappa = K_g^2 K_N, \quad (25)$$

where K_N (m^{-2} s^{-1}) is the rate of nucleation and K_g ($m\ s^{-1}$) is the linear rate of growth of the circular U_3O_8 islands. It was found that the rate expression developed by McEachern et al. [197] is an appropriate model for the two-dimensional nucleation and growth of U_3O_8. Moreover, their expression yielded a linear Arrhenius plot for the composite rate constant, k, so that they were able to extrapolate their high temperature (170–300°C) data to lower temperatures, more relevant to the dry air storage of used nuclear fuel. The slope of this plot corresponded to an activation energy of 146 ± 10 kJ mol^{-1}.

Nucleation-and-growth models, like those developed by Johnson and Mehl [38,39] and by McEachern et al. [197] are useful for assessment of U_3O_8-formation kinetic data. However, they are clearly only approximate models for a multifarious process that is replete with nuances. In particular, both of these nucleation-and-growth models assume that the rate of nucleation is constant, per unit of unreacted volume (or surface area, in the two-dimensional case). More sophisticated models could include multistep nucleation, time-dependent nucleation, or grain-size limitation on the size of U_3O_8 islands [198]. However, such models are probably of limited use until better experimental techniques are developed, to monitor the nucleation process during the course of reaction.

In the nucleation-and-growth model, the surface of a UO_2 sample is oxidized to U_3O_7 almost immediately and then U_3O_8 nucleation occurs on the U_3O_7 layer. The rate of nucleation is assumed to be proportional to the surface area of unreacted material. After a U_3O_8 nucleus has formed, its rate of growth is assumed to be isotropic and constant. The formation and subsequent growth of U_3O_8 nuclei continues until the degree of bulk oxidation approaches completion, and the fraction converted to U_3O_8 approaches unity. The general shape of a reaction curve obtained with the Johnson and Mehl equation is shown in Fig. 1(b). Aronson et al. [1] and Walker [35] found that the Johnson and Mehl model fits the oxidation data well and there is general agreement that this is an appropriate model for the oxidation of coarse powders and sintered pellets [28,35,187]. Note, however, that Harrison et al. [5] oxidized UO_2 microspheres (both irradiated and unirradiated) and found that the reaction kinetics, although sigmoidal, did not fit the Johnson and Mehl model. Possibly their kinetic data were influenced by relatively rapid grain-boundary oxidation in their samples.

Although the U_3O_8 nucleation-and-growth model is generally accepted, the details of the nucleation process remain unclear. Many workers have speculated that the formation of U_3O_8 nuclei does not begin immediately during oxidation but rather that the initial induction period observed for the oxidation of sintered UO_2 pellets corresponds only to the formation of U_3O_7/U_4O_9 [9,134,199]. It has also been suggested that the formation of cracks associated with the volume change of Eq. (13) leads to the formation of U_3O_8 nuclei [17,159,168,199]. Microscopic stresses on the UO_2/U_3O_7 sample surface may well play a role in U_3O_8 nucleation; Ohashi et al. [187] reported that annealing at 200°C delays the nucleation process significantly. Moreover, it has been shown that the rate of U_3O_8 nucleation on the surface of polished UO_2 pellets is related to the surface roughness [10].

The temperature-dependence of the nucleation process is also poorly understood. Aronson et al. [1] reported that fine powder displays a slower rate of nucleation (which was temperature-dependent) than coarse powders and thus speculated that the activation energy for the nucleation process is higher than that of U_3O_8 growth. In contrast, Walker [35] reported that the rate of nucleation is constant over the range 250 to 360°C.

Clearly, further study is required to elucidate the mechanism of U_3O_8 nucleation and the temperature-dependence of the nucleation process. Such information will be required to ascertain the validity of extrapolating U_3O_8-formation kinetic data obtained at high (200 to 300°C) temperatures to conditions relevant to the dry-air storage of used nuclear fuel (< 170°C).

The kinetics for the formation of U_3O_8 on UO_2 powders is more complex than for sintered pellets because of

overlap between the first and second stages of oxidation. Walker [35] found that fine UO_2 powders (2.6 to 3.6 $m^2\ g^{-1}$) oxidized according to parabolic kinetics at low temperatures (143 to 211°C), whereas single-crystal powders (0.0405 $m^2\ g^{-1}$) and sintered UO_2 specimens did not oxidize significantly until higher temperatures (250 to 360°C) and then displayed sigmoidal reaction kinetics. The overlap of the first and second stage of oxidation in powders has also been reported by Boase and Vandergraaf [28] and Takeuchi and Saito [154]. Comparison of the kinetic behaviour of unirradiated powders and pellets led Boase and Vandergraaf [28] to suggest that U_3O_8 can be formed both from U_3O_7 (on the surface) and directly from the bulk UO_2. However, such a mechanism is unlikely, because XRD analysis of the oxidation products of UO_2 sintered pellets generally displays small, but significant quantities of U_3O_7 prior to and concomitant with, the formation of U_3O_8 [9,10,134,199]. More plausible is the explanation that the layer of U_3O_7 that forms on sintered UO_2 is very thin, relative to the specimen dimensions, so that only small weight gains are observed prior to the nucleation and growth of U_3O_8.

The situation with used fuel is more nebulous than with unirradiated pellets. Bennett et al. [199] and Wood and Bannister [168] oxidized used AGR fuel fragments in air at 225 to 400°C and observed sigmoidal reaction kinetics. In contrast, You et al. [36,37] found that oxidation of used LWR pellet fragments displays parabolic kinetics at 300 to 400°C although unirradiated pellets followed sigmoidal kinetics (250 to 400°C). Similar findings were obtained at 230°C by Campbell et al. [18]. Wood et al. [200] also reported that the weight-gain curve for used AGR fuel is less clearly sigmoidal than the analogous curves obtained for unirradiated UO_2. Convolution of the first and second stages of oxidation is likely significantly different for used fuel than unirradiated material because of the relatively rapid rate of oxygen diffusion along grain boundaries in the former. Moreover, the U_3O_8 induction time for used fuel can differ from that of unirradiated UO_2 (Section 4.2). There is, however, no compelling evidence to suggest that the mechanism of the second stage of oxidation in used fuel is any different from that in unirradiated UO_2.

3.4. Models for the oxidation of UO_2 in defective fuel elements

The kinetics of air oxidation of used fuel have been studied extensively because of the need to predict the behaviour of defective fuel elements during air storage. Such calculations are difficult because of the complex nature of used fuel and the resulting models have thus been consistently complicated.

One feature of used-fuel oxidation that complicates mathematical modelling is the rapid rate of oxygen diffusion along grain boundaries relative to intragranular diffusion. Olander [201] developed a model for oxygen transport in used UO_2 that includes both lattice and grain-boundary diffusion. Application of this model to the low-temperature oxidation of individual used LWR fuel fragments by Einziger and Woodley [162] was successful. Stout et al. [202] modified Olander's dual-diffusion model by use of a density function, which describes the grain-boundary area per unit volume in the used-fuel fragments. Such a statistical approach allows one to model fuel oxidation for a wide range of fragment and grain sizes. Stout et al. [202] obtained good agreement between their model and experimental data obtained for the limiting case of small fragments. In addition, they were able to correlate their model with empirical expressions for UO_2 oxidation and, hence, to provide physical insight into the empirical rate constants.

Garisto [203] modelled the oxidation of UO_2 in a defective fuel element using an equivalent porous-medium representation for the cracked fuel. The oxidation process was assumed to be equivalent to a homogeneous reaction, and the rate was estimated by considering the bulk rate of weight gain, which is available from experimental data [21]. He solved the reaction-diffusion differential equations for both zeroth and first order with respect to oxygen concentration (the former of which corresponds to experimental results described by Tucker [42]). The resulting expressions qualitatively modelled the oxidation of defective fuel elements, but the predicted rate of oxidation was 170 times smaller than observed in the CEX-1 experiments [94]. Recently, Kolar [204] used the integral method to solve the zeroth-order reaction-diffusion model. By using recent kinetic data [93] for the rate of UO_2 oxidation, Kolar was able to obtain good agreement between calculated and experimental rates of progression of the oxidation front into defective CANDU elements stored in an unlimited air supply.

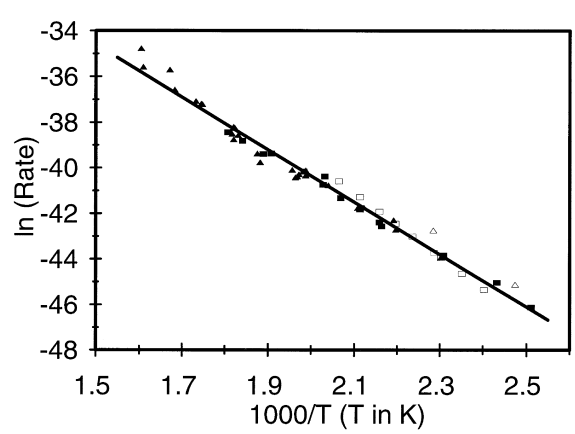

Fig. 5. Arrhenius plot for the diffusion-controlled parabolic rate constant for the formation of U_3O_7/U_4O_9 on UO_2. References for the various data are: ■ Blackburn et al. [4]; □ Walker [35]; ▲ Aronson et al. [1] and △ Anderson et al. [54].

Table 3
Published estimates of the activation energy for the diffusion-controlled formation of U_3O_7/U_4O_9 on unirradiated UO_2

Investigator	Material	Temperature range (°C)	E_{act} (kJ mol^{-1})
Anderson et al. [54]	UO_2 powder	131–164.5	104[a]
Aronson et al. [1]	UO_2 powder	161–350	102[a]
Blackburn et al. [4]	UO_2 pellets and powder	125–280	90.8
Walker [35]	UO_2 powder	143–211	120 ± 8

[a]Activation energy recalculated from investigators original data using the discrete-layer kinetic model (rather than the concentration-gradient model)

3.5. Activation energy for the formation of U_3O_7/U_4O_9

As discussed in Section 3.2, the formation of U_3O_7 on UO_2 powders obeys parabolic kinetics, whereas linear behaviour is observed for the oxidation of unirradiated, sintered UO_2 pellets. Kinetic data for the two types of models (parabolic and linear) for U_3O_7 formation are thus presented separately. Because literature data on the activation energy for the formation of U_3O_7/U_4O_9 have recently been critically reviewed by McEachern [62], the results are presented only briefly herein.

3.5.1. Parabolic kinetic data

Parabolic kinetic data have been typically fitted to an equation such as Eq. (15). Values of the parabolic rate constant (k) thus calculated have been tabulated by McEachern [62] and the results are shown as an Arrhenius plot in Fig. 5. In addition, the results published by Anderson et al. [54] and Aronson et al. [1] were converted by McEachern [62] from the concentration-gradient model that they used, to the discrete-layer model and these rate-constant data are also displayed in Fig. 5.

3.5.1.1. The data of Anderson et al. Anderson et al. [54] studied UO_2 oxidation by measuring the pressure drop associated with U_3O_7 formation. Data were fitted to the expression

$$\Gamma = K\sqrt{t} + A, \tag{26}$$

where Γ is the measured consumption of oxygen gas in cm^3 (STP [12]) g^{-1}, t is the time in min and K and A are empirically determined rate constants. McEachern [62] was able to show that the pressure-drop data can be converted to an effective thickness of the U_3O_7 oxide layer, and thence calculate the parabolic rate constant (Eq. (15)) for the data of Anderson et al. [54]. These data are included in the Arrhenius plot shown in Fig. 5.

Anderson et al. [54] reported UO_2 oxidation kinetic data for a variety of pressures between 0.003 and 65.3 kPa. Their data suggest that there is a significant influence of oxygen pressure on the rate of oxidation; thus McEachern [62] only included kinetic data for experiments performed with an oxygen pressure of 16 kPa (as an approximation to oxidation in air).

3.5.1.2. The data of Aronson et al. One of the seminal papers on UO_2 oxidation was published 40 years ago by Aronson et al. [1], who oxidized finely powdered UO_2 in dry air in the range 159 to 350°C. Unfortunately, their results were published before there was widespread acceptance of the discrete-layer mechanism for U_3O_7 formation [4]. Thus Aronson et al. [1] fitted their data to Eq. (14) for U_3O_7 formation along a concentration gradient.

Kinetic data were reported in terms of D, the oxygen diffusion coefficient and r, the radius of the initial UO_2 particle. The kinetic data reported by Aronson et al. [1] were converted by McEachern [62] to rate constants by using Eq. (14) to calculate the time required for 50% reaction (i.e. $C = 0.5$). The discrete-layer mechanism rate constant, k, was then calculated by using these values of C and t in Eq. (15).

The results of the kinetic data converted to the discrete-layer model are included in Fig. 5; the calculated activation energy was 102 kJ mol^{-1} (Table 3).

3.5.1.3. The data of Blackburn et al. Blackburn et al. [4] were among the first to examine the kinetics of U_3O_7 formation in detail. They measured the rate of weight gain for UO_2 powders and wafers excised from unirradiated UO_2 fuel pellets. They reported that parabolic kinetics were observed in the early stages (up to 1% conversion) of the reaction for the sintered pellets. Most of the data reported by Blackburn et al. [4] were measured in oxygen at a pressure of 10 kPa; however, they did not find a dramatic effect on oxidation rate between 10 and 101 kPa of O_2. They fitted their kinetic data to Eq. (15) and derived an estimate of 90.8 kJ mol^{-1} for the formation of U_3O_7; their kinetic data are included in Fig. 5.

3.5.1.4. The data of Walker. Walker [35] gravimetrically measured the rate of oxidation in air of both powders and pellets of unirradiated UO_2. He reported that the kinetic data could be fitted to either Eqs. (14) and (15). Values of the rate constant, k, were not reported for individual temperatures; rather, values of the pre-exponential factor,

[12] Standard temperature (273.15 K) and pressure (101.325 kPa).

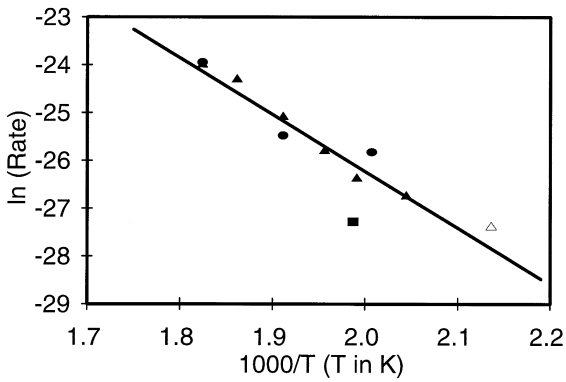

Fig. 6. Arrhenius plot for the linear rate constant for the formation of U_3O_7/U_4O_9 on sintered UO_2. References for the various data are: ■ Tempest et al. [57]; ● Smith [63]; ▲ Taylor et al. [44] and △ Thomas and Einziger [12].

k_o, and the activation energy, E_a, were given for the Arrhenius expression

$$k = k_o e^{-E_a/RT}. \quad (27)$$

To compare Walker's kinetic data with those discussed herein, the value of k was calculated from Eq. (27) for the finely divided (radius = 0.1 μm) UO_2 powder described in his Fig. 1, for each temperature shown therein. Calculated values of the oxidation rate constant, k, based on Walker's data yielded an activation energy of 120 ± 8 kJ mol^{-1}; these results are included in Fig. 5.

3.5.1.5. Summary of diffusion-controlled kinetic data. Values of the parabolic rate constant, k, calculated from the kinetic data presented by various investigators [1,4,35,54] were tabulated by McEachern [62] and are displayed as an Arrhenius plot in Fig. 6. A linear regression was performed on the data displayed in Fig. 6 and gave the following Arrhenius relation for the parabolic rate constant:

$$\ln(k) = -\frac{95.7 \text{ kJ mol}^{-1}}{R}\frac{1}{T} - 17.33. \quad (28)$$

The calculated activation energy of 96 kJ mol^{-1} is lower than most of the values reported in Table 3. However, the consistency between the activation energy calculated herein and the data published earlier (Table 3) is reasonably good considering the range of sample types and experimental techniques used in the earlier studies.

3.5.2. Linear kinetic data

As noted in Section 3.2, the rate of U_3O_7 formation on unirradiated sintered UO_2 pellets often displays linear kinetic behaviour. Linear rate constants (k') from the following four studies are compiled in Table 4.

3.5.2.1. The data of Smith. Smith [63] studied the rate of oxidation of unirradiated UO_2 pellets by measuring the decrease in oxygen pressure associated with the reaction. He reported that the quantity of U_3O_7 increases linearly with time and interpreted this to mean that the reaction was diffusion controlled through a constant-thickness product layer (i.e. that oxygen diffusion through UO_2 is faster than through U_3O_7). Kinetic data measured by Smith were for 80 kPa of O_2 but are likely applicable to air oxidation, since the rate of oxidation is not strongly dependent on oxygen partial pressure above ~20 kPa [4].

3.5.2.2. The data of Taylor et al. Taylor et al. [44] measured the rate of formation of U_3O_7 on the surface of polished disks, cut from unirradiated CANDU fuel pellets, by quantitative analysis of the XRD patterns. Samples oxidized in laboratory air in the range 216 to 275°C displayed linear rates of U_3O_7 growth in the early stages of the reaction.

Table 4
Linear rate constant (k') for the first stage of UO_2 oxidation

Investigator	Sample	Method	Temperature (°C)	k' (m s^{-1})
Taylor et al. [44]	sintered UO_2 pellets	XRD	216	2.5×10^{-12}
			229	3.6×10^{-12}
			238	6.4×10^{-12}
			250	1.3×10^{-11}
			264	2.86×10^{-11}
			275	3.89×10^{-11}
Tempest et al. [57]	sintered UO_2 pellets	XRD	230	1.42×10^{-12}
Smith [63]	sintered UO_2 pellets	ΔP	225	6.1×10^{-12}
			250	8.6×10^{-12}
			275	3.97×10^{-11}
Thomas and Einziger [12]	used LWR fuel	SEM	195	1.31×10^{-12}

3.5.2.3. The data of Tempest et al. Tempest et al. [57] measured the rate of U_3O_7 formation on the surface of planchets excised from unirradiated AGR fuel pellets and subsequently oxidized in air at 230°C. Quantitative analysis of the XRD patterns showed that the thickness of the U_3O_7 layer increases linearly with time at a rate of 1.42×10^{-12} m s^{-1}.

3.5.2.4. The data of Thomas and Einziger. Thomas and Einziger [12] studied the formation of U_4O_{9+y} on used LWR fuel by the anomalous electron backscattering SEM technique. They reported that at 195°C the thickness of the U_4O_{9+y} layer increases linearly with time in the early stages of the reaction, i.e. for samples oxidized to compositions between $UO_{2.04}$ and $UO_{2.16}$. The reported value for the rate of intragranular oxidation was 4.7 nm h^{-1}, or 1.31×10^{-12} m s^{-1}.

3.5.2.5. Summary of the linear kinetic data. Linear kinetic behaviour in the first stage of the oxidation of sintered UO_2 pellets is clearly an approximation resulting from a multifarious process involving cracking and both grain-boundary and intragranular oxidation. There is thus no obvious reason to expect Arrhenius behaviour to be observed for the linear kinetic data. Nonetheless, an Arrhenius plot (Fig. 6) displays reasonably good linear behaviour. Linear regression of the data displayed in Fig. 6 gives the expression

$$\ln(R) = -\frac{98.6 \text{ kJ mol}^{-1}}{R}\frac{1}{T} - 2.513 \qquad (29)$$

The calculated activation energy of 98.6 kJ mol^{-1} is very similar to the value of 95.7 kJ mol^{-1} derived from diffusion-controlled kinetic data in Section 3.5.1.5. The similarity between the two activation energies may suggest that the rate of oxygen diffusion dominates the kinetic expression for the rate of oxidation of sintered UO_2 pellets.

3.5.3. Activation energy for the formation of U_3O_7/U_4O_9 on used fuel

The activation energy for the formation of U_3O_7/U_4O_9 on used fuel is of great practical importance; however, there is much less information on oxidation of used fuel than unirradiated UO_2 because of the technical difficulties involved.

3.5.3.1. The data of Woodley et al. Woodley et al. [93,205] oxidized fragments of used LWR fuel in air in the range 140 to 225°C and measured the extent of oxidation by weight gain. They reported that oxidation proceeds by migration along the grain boundaries and then by intragranular progression of a layer of U_4O_{9+y}. McEachern [62] was thus able to calculate values of the parabolic rate constant, k, by assuming that the effective particle size, r, used in Eq. (15) was the grain size of the initial UO_2.

Woodley et al. [93] found that the experimentally determined rate constants are a function of the degree of oxidation and that a true steady-state value of k is only obtained at $\Delta(O/M)$ values of ~ 0.1 or greater. McEachern [62], therefore, used the data corresponding to $\Delta(O/M) = 0.11$ reported by Woodley et al. [205] for calculation of the diffusion-controlled rate constant, k. The values of k were calculated using Eq. (15) with values of $r = 9.3 \times 10^{-6}$ m and $a = 0.99$. The results of such calculations yielded an estimate of 113 ± 17 kJ mol^{-1} for the activation energy for the formation of U_3O_7 on used LWR fuel.

3.5.3.2. The data of Einziger et al. Einziger et al. [120] studied the rate of U_4O_{9+y} formation by using an SEM imaging technique to measure directly the rate of intragranular growth of the oxide layer. Used-fuel fragments and coarse powders from LWR reactors were oxidized at 175 and 195°C in air. The samples did not display completely uniform oxidation; however, the authors were able to study the oxidation kinetics in those regions of the samples that displayed uniform rates of intragranular oxidation. The kinetic data suggested that U_4O_{9+y} formation obeys parabolic kinetics. The rate constant, k, was found to be 1.11×10^{-19} and 3.50×10^{-19} m^2 s^{-1} at 175 and 195°C, respectively, which yields an activation energy of 100 kJ mol^{-1}.

3.5.3.3. Summary of data on the activation energy for U_3O_7/U_4O_9 formation on used fuel. The activation energy for the formation of U_3O_7/U_4O_9 on used fuel is estimated by taking the average of the values reported by Einziger et al. [120] and Woodley et al. [93,205]. The resulting value of 106 kJ mol^{-1} is somewhat higher than the value of 96 kJ mol^{-1} calculated in Section 3.5.1.5 for diffusion-controlled formation of U_3O_7 on UO_2 powders. There are few data for used fuel, however, so it is difficult to ascertain whether the differences between UO_2 and used fuel are significant.

3.6. Activation energy for the formation of U_3O_8

3.6.1. Unirradiated UO_2

Much of the early work [1,35,132] on the formation of U_3O_8 was done by measuring the weight gain throughout the oxidation process and then fitting the data to a standard model for solid-state reaction kinetics. Models for the rate of U_3O_8 formation include the Johnson–Mehl (Eq. (22)) and Avrami–Erofeev equations (Eq. (23)).

Aronson et al. [1] oxidized UO_2 powders and fitted their kinetic data to Eq. (22). They estimated the rate of U_3O_8 nucleation and assumed that the ratio of the rate of nucleation, relative to that of U_3O_8 growth, was constant over the temperature range studied (278 to 325°C). Aronson et al. [1] were then able to derive an estimate of 146 kJ

mol^{-1} for G, the rate of growth of U_3O_8 nuclei on UO_2 powders.

Walker [35] studied the oxidation of both UO_2 powders and sintered pellets and fitted his weight-gain data to the Johnson–Mehl model (Eq. (22)). He claimed that the shape of the reaction curve could be used to estimate the rate of U_3O_8 nucleation. Moreover, he stated that the rate of nucleation is constant over the temperature ranges studied (312 to 352°C for powders and 279 to 361°C for pellets). The kinetic data gave values of the activation energy for the growth of U_3O_8 of 134.7 kJ mol^{-1} for powders and 110.5 kJ mol^{-1} for pellets.

Saito [132] oxidized UO_2 powders in the range 315 to 360°C and reported that the oxidation process could be fitted to Eq. (23) with $n = 3$. He thus obtained an activation energy of 127.6 kJ mol^{-1} for the formation of U_3O_8.

All of the above studies were based on the fitting of kinetic data to a standard reaction model and the use of assumptions on the rate of U_3O_8 nucleation. To derive an activation energy for U_3O_8 growth, Walker [35] assumed that the rate of nucleation was independent of temperature. In contrast, Aronson et al. [1] and Saito [132] implicitly assumed that the rate of nucleation and growth have the same temperature dependence; they thus calculated activation energies that represent a composite for both the nucleation and growth of U_3O_8. The assumptions on the rate of U_3O_8 nucleation, which were used in the early studies [1,35,132], were not clearly justified. Moreover, the oxidation of UO_2 is, in general, a two-stage process [1,4], and it is difficult to ascertain the extent to which the formation of the intermediate U_3O_7 interferes with weight-gain data on the rate of U_3O_8 formation.

Boase and Vandergraaf [28] studied unirradiated UO_2 pellets, and found that the relative rates of nucleation and growth are not constant over the temperature range of their experiments (320 to 460°C), and they thus recognized that their calculated activation energy of 96 kJ mol^{-1} is of questionable validity. Therefore, rather than using the Johnson and Mehl model [38,39] and making assumptions about the rate of nucleation, they plotted the time for 5, 10 and 50% conversion to U_3O_8 and calculated 'pseudo-activation energies'. An Arrhenius plot of the time required to reach 5, 10 and 50% conversion to U_3O_8 displayed similar behaviour for each percentage transformed, with two distinct regions in the Arrhenius plot. In the range 330 to 350°C the pseudo-activation energy was 170 kJ mol^{-1}, whereas it was 67 kJ mol^{-1} in the range 350 to 450°C. Tests on unirradiated powders gave a similar Arrhenius plot with two linear regions; the calculated pseudo-activation energy based on the time-to-50% reaction was 163 kJ mol^{-1} in the region 200 to 350°C. Measurements [28] of the rate of progression of the oxidation front into a defective, unirradiated element gave qualitatively similar results and activation energies of 172 kJ mol^{-1} at 250 to 300°C and 62.8 kJ mol^{-1} at 300 to 350°C.

Boase and Vandergraaf [28] reported their results as 'pseudo-activation energies' because the time required to reach a given percent conversion to U_3O_8 is not necessarily inversely proportional to the rate of reaction. Specifically, approximation of the reaction rate with the inverse of the time required to reach a given percent reaction will introduce an error if the reaction kinetics are not linear with time. If there is a significant induction time for the reaction, as is often observed with U_3O_8 formation [4], then the pseudo-activation energies reported by Boase and Vandergraaf will differ from the actual activation energy for U_3O_8 formation. However, the data reported by Boase and Vandergraaf are of immense practical importance, and their use of two activation energies (over different temperature ranges) has proven correct. It has now been clearly shown [9,42,168] that there are at least two different activation energies (at different temperature ranges) for the formation of U_3O_8, with a change in oxidation behaviour around 300 to 350°C. Thus the results of Saito [132] and Walker [35] are likely an average activation energy for the two different mechanisms.

White et al. [135] measured the rate of weight gain per unit surface area for LWR pellets oxidized in air between 200 and 250°C. They reported that the kinetic behaviour before the initiation of U_3O_8 spallation was different from that observed once U_3O_8 powder formation had begun. The activation energy was found to be 102 kJ mol^{-1} prior to the onset of spallation, and 160 kJ mol^{-1} in the post-spallation period. The pre-spallation kinetic data likely represent the superposition of U_3O_7 formation on both the nucleation and growth of U_3O_8. The post-spallation activation energy reported by White et al. [135] likely corresponds to the formation of U_3O_8, but these data may have significant error associated with the change in surface area that occurs when powder formation begins.

You et al. [36,37] measured the weight gain of portions of LWR pellets and observed sigmoidal reaction curves. They estimated the activation energy for the formation of U_3O_8 on UO_2 to be 143 kJ mol^{-1} in the range 250 to 350°C and 109 kJ mol^{-1} in the range 350 to 400°C using an Arrhenius plot of the time-to-50% reaction. Their results are, thus, comparable with the pseudo-activation energies reported by Boase and Vandergraaf [28] but are not directly comparable with the related work reported by White et al. [135]. A more recent paper from the same Korean research group [22] gives an estimated activation energy of 145 kJ mol^{-1}, based on an Arrhenius plot of the onset time for U_3O_8 formation (as detected by XRD) at temperatures between 150 and 300°C.

Tucker [42] measured the rate of oxidation of portions of AGR pellets gravimetrically in controlled atmospheres (O_2 content varying between 0.1% and 27%). At temperatures below 500°C, he found sigmoidal reaction kinetics. An activation energy for the post-induction period was determined by describing the reaction kinetics in terms of a maximum linear rate of weight gain and using these data

to construct an Arrhenius plot. The linear approximation to the sigmoidal reaction kinetics was found to give an activation energy of 170.2 kJ mol^{-1} in the range 200 to 300°C and 48.0 kJ mol^{-1} in the range 300 to 550°C. The results reported by Tucker [42] have significant errors because the rate of spalling of U_3O_8 from the sample surface affects the reaction kinetics and because linearity is a fairly poor approximation to the sigmoidal reaction kinetics.

The focus of this paper is the determination of the activation energy for the formation of U_3O_8 at low temperatures (i.e. < 300°C), since this is the range of interest for the dry storage of used nuclear fuel. We thus only mention briefly the activation energy of ~ 100 kJ mol^{-1} reported by Ohashi et al. [7] for the temperature range 300 to 450°C and the value of 161.5 kJ mol^{-1} determined by Kissinger's method [206] for the range 365 to 400°C [109].

Taylor et al. [10] studied the early stages of U_3O_8 formation on the surface of unirradiated UO_2 sintered pellets in the temperature range 200 to 300°C. They used XRD to determine the progress of U_3O_8 formation because this technique measures U_3O_8 specifically, i.e. without interference from the intermediate U_3O_7 phase. Arrhenius plots were made based on the time required for the production of 'minor' or 'detectable' amounts of U_3O_8 and this semi-quantitative procedure yielded estimated activation energy values of 139 and 124 kJ mol^{-1}, respectively.

In conclusion, the activation energy for the formation of U_3O_8 has been widely studied (Table 5), but it appears that the U_3O_8-formation process is not yet well understood. Three separate approaches have been used to estimate the activation energy for U_3O_8 formation:

(1) Fitting kinetic data to a nucleation-and-growth model and making assumptions on the relative rates of nucleation and growth as a function of temperature.

(2) Calculating the activation energy based on an empirical 'time-to-50% reaction', as performed by Boase and Vandergraaf [28] and You et al. [36]. The data given by Taylor et al. [10], which were based on the time required for the formation of 'minor' and 'trace' amounts of U_3O_8, fit into this category of empirical pseudo-activation energy calculations.

(3) By assuming that the rate of reaction during the linear portion of the sigmoidal reaction kinetics is strictly the result of U_3O_8 growth. This is not a particularly good approximation, because the linear portion of the sigmoidal reaction curve is a convolution of both nucleation and growth kinetics. In addition, weight-gain experiments may have additional errors associated with the concurrent formation of U_3O_7, particularly for powdered samples.

None of the above methods is truly satisfactory for describing the kinetics of the formation of U_3O_8 because in each case several assumptions have been made or the kinetics of the nucleation and growth stages for U_3O_8 have

Table 5
Published estimates of the activation energy for the formation of U_3O_8 on UO_2 and used fuel

E_{act} (kJ mol^{-1})	Sample	Temp. range (°C)	Method	Ref.
146	UO_2 powder	278–325	gravimetric	[1]
127.6	UO_2 powder	315–360	gravimetric	[132]
~ 100[a]	UO_2 microspheres	300–450	gravimetric	[7]
161.5	UO_2 powder	365–400	DTA	[109]
134.7	UO_2 powder	312–352	gravimetric	[35]
110.5	UO_2 pellets	279–361	gravimetric	[35]
170.2	AGR pellet fragments	200–300	gravimetric	[42]
48	AGR pellet fragments	300–550	gravimetric	[42]
124–139	CANDU pellets	200–300	XRD	[10]
102[b]	LWR pellets	200–250	gravimetric	[135]
163	UO_2 powder	200–350	gravimetric	[28]
170	CANDU pellets	330–350	gravimetric	[28]
67	CANDU pellets	350–450	gravimetric	[28]
172	CANDU fuel element	250–300	progression of oxidation front	[28]
63	CANDU fuel element	300–350	progression of oxidation front	[28]
143	UO_2 pellet fragments	250–350	gravimetric	[36]
109	UO_2 pellet fragments	350–400	gravimetric	[36]
94.5	used LWR fuel	300–400	gravimetric	[36]
140	unirradiated CANDU fragments	175–400	gravimetric	[21]
120	irradiated CANDU fragments	175–400	gravimetric	[21]
194	used LWR fragments	250–360	visual exam.	[207]

[a] The activation energy was observed to vary as a function of oxygen pressure.
[b] The value of 102 kJ mol^{-1} corresponds to the oxidation prior to powder formation. The post-spallation period displayed an activation energy of 160 kJ mol^{-1}.

not been properly deconvoluted. However, the studies described above provided the best estimates so far for the activation energy for U_3O_8 formation, and we have used them to obtain a recommended average value for the combined (nucleation and growth) activation energy for temperatures below ~325°C. We include in the average the three values reported by Boase and Vandergraaf [28], namely 170 kJ mol^{-1} for UO_2 pellets, 163 kJ mol^{-1} for powder, and 172 kJ mol^{-1} based on oxide front progression, together with the two values reported by Taylor et al. [10], and the single values reported by Aronson et al. [1], Tucker [42], White et al. [135] and You et al. [36]. The resulting average activation energy is 154 kJ mol^{-1}. Note that the value and units of the pre-exponential term, needed to derive a rate constant from this activation energy, depend on which of the three approaches, outlined above, is used.

The calculated average value for the activation energy for U_3O_8 formation is a legitimate first approximation for modelling UO_2 oxidation. However, the use of an average activation energy for both the nucleation and growth kinetics is not an ideal situation, especially given that the dry-air storage of used nuclear fuel is modelled based on the extrapolation, to temperatures below 150°C, of data obtained at higher temperatures (200 to 325°C). In fact, nucleation probably does not follow Arrhenius kinetics at all [208]. Clearly, more study is required to fully understand this complex and important area.

3.6.2. Used fuel

Several values have been reported for the activation energy for the formation of U_3O_8 on used UO_2 fuel (Table 5). Bennett et al. [199] measured the rate of weight gain of individual fragments of used AGR fuel. They did not report an activation energy but showed an Arrhenius plot with two linear regions, one region from 225 to 300°C and another from 350 to 400°C. The derived rate expressions correspond to activation energies of 155 and 81.0 kJ mol^{-1}, respectively. You et al. [36,37] measured the rate of weight gain of individual used LWR fuel fragments at 300 to 400°C and reported an activation energy of 94.5 kJ mol^{-1} for the formation of U_3O_8 on UO_2. Hastings and coworkers performed similar weight-gain experiments on fragments of used CANDU fuel [21,209]. They claimed that a linear Arrhenius plot is valid over the range 175 to 400°C and suggested that deviations from linearity in previous work may be related to oxygen starvation at higher temperatures. The activation energy for U_3O_8 formation was estimated to be 120 kJ mol^{-1} for used CANDU fuel. However, it seems doubtful that their interpretation of linear Arrhenius behaviour over such a wide temperature range is valid [9,28,42,168,200] and the importance they attach to oxygen starvation has been questioned [42,168]. Harrison et al. [5] oxidized irradiated polycrystalline UO_2 spheres and reported that the reaction proceeds by two stages; however, they were careful to point out that their 'second stage' need not correspond to the reaction $U_3O_7 \rightarrow U_3O_8$. They reported that the activation energy for the second stage of the reaction is a function of burnup. In the temperature range 320 to 380°C, they found an activation energy of 63 kJ mol^{-1} for low burnups, ranging up to 105 kJ mol^{-1} for high burnups (9 at.%). Einziger and Strain [207] oxidized used LWR fuel fragments in air in the range 250 to 360°C and recorded the time when spallation began. They found that the time-to-spallation displayed Arrhenius behaviour with an activation energy of 194 ± 24 kJ mol^{-1}.

Because UO_2 oxidation proceeds by two steps (and the second stage has an induction period), the overall reaction is complex, and thus there are potential problems with the application of weight-gain data to the study of the reaction kinetics. Estimation of the activation energy for the formation of U_3O_8 from weight-gain data is only valid in the case where the quantity of the intermediate U_3O_7/U_4O_9 is insignificantly small or where the data are fitted to an expression that takes into consideration the complex nature of the oxidation reaction. For unirradiated UO_2, the rate of U_3O_7/U_4O_9 formation was often small relative to the rate of U_3O_8 formation, especially for sintered pellets, which have a low specific surface area. However, for used fuel the rate of U_3O_7/U_4O_9 formation is fast because of rapid grain-boundary diffusion [58]. The approximation that the quantity of U_3O_7/U_4O_9 is small in used-fuel oxidation experiments is thus of questionable validity at temperatures below 250°C; for example, Thomas et al. [45] did not observe U_3O_8 in used LWR fuel samples oxidized up to compositions near $UO_{2.4}$ below 250°C. In fact, low-temperature weight-gain curves for used-fuel fragments often reach a plateau near 2% weight gain [36,207], which suggests that U_3O_7/U_4O_9 may be the dominant phase. Similarly, Wasywich et al. [16] noted that defective CANDU fuel elements oxidized in limited air at 150°C show substantial quantities of U_3O_7 near defects. Under these conditions, only minor quantities of U_3O_8 are slowly formed (Wasywich and Taylor, unpublished observations). We thus conclude that the data of Bennett et al. [199] for 225 to 300°C and that of Hastings and co-workers [21,209] for 175 to 400°C likely represent a combination of two different activation energies (i.e. for the formation of U_3O_7/U_4O_9 and also of U_3O_8), because they did not consider the fact that two separate reactions are occurring in the temperature ranges studied. Clearly, the lack of any reliable estimate of the activation energy for the formation of U_3O_8 on used fuel, at temperatures relevant to dry-air storage, is a major concern that should be addressed in order to define upper limits for storage temperatures.

The high-temperature data of Bennett et al. [199], Harrison et al. [5] and You et al. [36,37] are apt to be more accurate than the low-temperature data, but it is possible that the formation of U_3O_7/U_4O_9 still introduces significant errors into such estimates of the activation energy for the growth of U_3O_8. An estimate of the activation energy for the formation of U_3O_8 on UO_2 above ~325°C can be

obtained by averaging the values reported by You et al. [36,37] and Bennett et al. [199], along with the value reported by Harrison et al. [5] for 1.45 at.% burnup. The resulting average value is 95 kJ mol^{-1}, which is within the range of values for unirradiated fuel at comparable temperatures (Section 3.6.1).

4. Differences in oxidation behaviour between unirradiated UO_2 and used fuel

4.1. Formation of U_3O_7/U_4O_9

It is generally accepted that the early stages of low-temperature (< 250°C) oxidation to U_3O_7/U_4O_9 occur more rapidly for used nuclear fuel than unirradiated, sintered UO_2 [18,19,21,23,28,199,200]. Typical comparisons of the reactivity of UO_2 with that of used fuel were performed on small (~ 1 g) fragments of material oxidized in air in the range 200 to 300°C. Such tests have shown that the rate of oxidation of unirradiated UO_2 fragments is slower than that of used fuel by a factor of 2 to 50 in this temperature range [19,21,23,36,199,200]. However, the rate of the first stage of oxidation (as indicated by weight gain) appears to be independent of fuel burnup in the range 8 to 34 MW d/kg U for used LWR fuel [18,20].

The rate of U_3O_7/U_4O_9 formation in used LWR fuel is rapid relative to that of unirradiated UO_2, partly because of the concentration of fission-product gas bubbles along grain boundaries [210]. The gas bubbles provide ready access of oxygen to the interior of the sample. Oxidation thus occurs first along the grain boundaries and formation of U_4O_{9+y} then proceeds into the individual UO_2 grains [45] as a discrete layer. Fragments taken from the outer portion of a fuel pellet display a uniform thickness of the U_4O_{9+y} layer throughout the sample because the rate of oxygen diffusion along the grain boundaries is fast relative to the rate of conversion to U_4O_{9+y}. The U_4O_{9+y} is more dense than UO_2, and thus its formation results in microcracking along the grain boundary, which further enhances the rate of oxygen ingress [13,58]. During irradiation, the centre of the fuel pellets is hotter than the outer regions, resulting in fewer (but larger) fission-gas bubbles along grain boundaries in the central region. The low connectivity of the large bubbles results in a relatively slow rate of oxygen migration along grain boundaries in fragments that originated from the pellet core. The oxidation process is thus non-uniform in some used LWR fuel specimens [13,45], as well as in used CANDU fuel [16].

The presence of significant quantities of fission products in solid solution in used UO_2 fuel changes the oxidation process so that the product of the first stage of oxidation resembles U_4O_{9+y} (i.e. it is cubic), rather than the tetragonal (or at least non-cubic) U_3O_7 observed after oxidation of undoped or unirradiated UO_2 [45]. Detailed studies have not yet been done, but it is likely that dissolved fission products in used fuel may be responsible for the different reactivity observed between unirradiated UO_2 and used fuel [18,43,63]. The effect of dopants on the oxidation process has been discussed in Section 2.3.

Data indicate that the γ-radiation associated with used fuel does not have a major impact on the rate of oxidation (Section 2.6) except possibly by NO_x production, which can result from radiolysis of the cover gas (Section 2.5).

4.2. Formation of U_3O_8

The second stage of the oxidation process

$$U_3O_7/U_4O_9 \rightarrow U_3O_8 \qquad (30)$$

occurs at a significant rate above ~ 250°C. Thus the overall rate of reaction (e.g. as measured in weight-gain experiments) above 250°C is more complex than was the case for low-temperature oxidation. Boase and Vandergraaf [28] found that powdered, used CANDU fuel oxidizes 3 to 3.5 times faster than unirradiated UO_2 powders between 200°C and 300°C; however, they observed no significant differences between the rates of oxidation of UO_2 pellets and used-fuel fragments at 320 to 460°C. Similarly, Hastings et al. [21] reported that irradiated CANDU fuel oxidizes two to three times faster than UO_2 at temperatures below 300°C, but that the reaction occurs at similar rates in the range 300 to 400°C. Simpson and Wood [9] reported only a modest effect of irradiation on the linear rate of U_3O_8 formation at 250°C for AGR fuel. Wood et al. [200] found that used AGR fuel oxidized faster than unirradiated UO_2 at temperatures below 300°C, whereas the rate of oxidation was the same at 300 to 400°C. Bennett et al. [199] reported that used AGR fuel oxidized faster than UO_2 by a factor of 2.

The bulk of the evidence thus suggests that below ~ 300°C the rate of used-fuel oxidation is significantly faster than that of unirradiated UO_2. In contrast, between 300 and 400°C there is no difference between the oxidation rate of used fuel and that of unirradiated UO_2. It therefore appears that the rapid rate of low-temperature oxidation of used fuel is due to the formation of U_3O_7/U_4O_9, which is enhanced by rapid oxygen diffusion along the grain boundaries and perhaps by radiation-enhanced oxygen diffusion. The formation of U_3O_8, along with concomitant spalling, dominates the oxidation kinetics above 300°C, and the data suggest that these processes are not significantly different for UO_2 and used fuel in this temperature range. Conversely, there does appear to be some inhibition of U_3O_8 formation in used LWR fuel below 250°C (see below).

Harrison et al. [5] described complex kinetic behaviour for the oxidation of used UO_2 fuel pellets. They found that conventional first-order kinetic plots display two distinct stages and that the activation energy of the second stage increases with burnup, although they carefully pointed out that the second stage of the kinetic plot does not necessarily correspond to Eq. (30). Similarly, Smith [63] found that the latter stages of the oxidation process for UO_2 doped

with fission products displayed a higher activation energy than for pure UO_2. It is possible that the formation of U_3O_8 in used fuel is delayed by the presence of fission products (Section 2.3); however, the effect is probably quite small [117].

From a fuel storage or disposal perspective, one of the most important parameters in the oxidation process is the time-to-powder, t_p (i.e. the time required for the production of U_3O_8 particulate). Despite its practical importance, the relationship between t_p and burnup remains poorly understood. Tests have shown that the time required for U_3O_8 powder formation is lower for some types of used fuel than for unirradiated UO_2. Bennett et al. [199] reported that the time-to-powder is shorter for used fuel than UO_2 by a factor of 7 at 175°C, but they found that there is essentially no difference in the respective values of t_p at 300°C. Similar, tentative results were reported by Simpson and Wood [9] and Wood et al. [200]. The dependence of t_p on burnup is not well understood. Bennett et al. [199] reported that there is no apparent relationship between t_p and burnup in the range 12 to 27 MW d/kg U. Similarly, Hastings and Novak [209] and Wood et al. [200], working with used CANDU and AGR fuel, respectively, did not find any obvious correlation between burnup and t_p. In contrast, Campbell et al. [18] and Gilbert et al. [20] reported that the time-to-powder at 230°C increased with burnup (8 to 34 MW d/kg U) for used boiling-water reactor (BWR) fuels. They also found that pressurized-water reactor (PWR) fuels powder more slowly than used BWR fuels, so that they were unable to correlate t_p with burnup in the former case. Olsen [211,212] reported qualitatively similar results from an oxidation experiment on a defective used BWR fuel rod, in which he found that diametral rod enlargement (because of U_3O_8 powder formation) occurred most quickly at the ends of the rod (which have the lowest burnup). Gilbert et al. [19,115] gave a plot of $\log(t_p)$ versus burnup for a series of samples oxidized in the range 220 to 283°C. They reported that there is in general a positive correlation between the burnup and t_p. The convolution of the rapid rate of weight gain in used fuel along with the burnup dependence of t_p may lead to a minimum in the plot of t_p versus burnup at low burnup levels [19]. Such behaviour may account for the lack of any obvious correlation between t_p and burnup, as reported by Hastings and Novak [209].

It now appears reasonably certain that the positive correlation between t_p and burnup reported for PWR fuel [19] is valid (at least for large burnups), although the reason for this behaviour is not entirely clear. Gilbert et al. [19] suggested that the slower rate of powder formation in used fuel may be attributed to burnup-enhanced diffusion rates for oxygen; that is, the rapid diffusion of oxygen into used-fuel particles prevents the rapid buildup of O/U ratios of 2.67 near the surface of the fuel, and thus U_3O_8 formation is hindered. However, Choi et al. [117] were able to replicate the burnup dependence of t_p using SIMFUEL, which has the fission-product content of used fuel but does not have extremely rapid grain-boundary diffusion rates for oxygen. The effect of fission products, present in the used fuel as a solid solution, may thus retard the formation of U_3O_8 in a manner similar to that reported for doped UO_2 (Section 2.3). Very recently, Kim et al. [22] have confirmed that the rate of formation of U_3O_8 at 275°C on high-burnup UO_2 (37 GW d/MTU) and Gd-doped UO_2 (10 and 27 GW d/MTU) fuels is much slower than on unirradiated UO_2 pellets, and that the rate on low-burnup UO_2 fuel (10 GW d/MTU) is intermediate between these extremes.

5. Overall summary and an approach to modelling fuel oxidation

It is evident from our review that the literature on the air oxidation of UO_2 is extensive, often repetitive and sometimes contradictory. It is therefore challenging to extract reliable kinetic data and devise a methodology for modelling the oxidation process in detail. Here, we offer a possible approach to this problem.

The main concern with fuel oxidation, from the viewpoint of irradiated fuel storage and disposal, is the formation of U_3O_8, or other high-volume phases, which can cause splitting of the cladding and powdering of the fuel. The formation of the U_3O_7/U_4O_9 intermediate is comparatively benign, although it causes the grain boundaries to open because U_3O_7/U_4O_9 has a 2% smaller molar volume than UO_2. Some understanding of U_3O_7/U_4O_9 formation is important, because the grain separation increases the surface area of fuel accessible to air oxidation. Also, it is possible that formation of this oxygen-rich fluorite-type phase is a necessary precursor to U_3O_8 nucleation.

There is, in general, good agreement that U_3O_7/U_4O_9 formation follows parabolic (diffusion-controlled) kinetics for the oxidation of powders and during the early stages of oxidation of unirradiated pellets. In the latter case, the reaction switches to linear kinetics as the U_3O_7/U_4O_9 layer thickens beyond a few tenths of a micrometre. Reported values of the activation energy for the parabolic kinetics for unirradiated UO_2 are fairly consistent, and the mean value of 96 kJ mol^{-1} is deemed reliable. There is rather less kinetic data for the diffusion-controlled oxidation of used fuel and the mean value of 106 kJ mol^{-1} is thus less certain than that of unirradiated fuel. The average activation energy for the linear kinetic regime of unirradiated pellets is 99 kJ mol^{-1}.

The kinetics of U_3O_7/U_4O_9 formation is reasonably well understood. The rate of grain boundary oxidation is the one parameter affecting the rate of U_3O_7/U_4O_9 formation that is difficult to describe quantitatively. For many irradiated light-water reactor fuels, grain-boundary oxidation is very fast (relative to intragranular oxidation) and oxidation thus proceeds uniformly throughout the fuel.

However, some irradiated LWR fuel samples oxidize non-uniformly, i.e. grain-boundary access is not uniform and immediate [13]. This also appears to be the case with irradiated CANDU fuel [16]. Grain-boundary penetration is much slower for unirradiated materials and indeed it is often not observed at all. One conservative approach to modelling fuel oxidation during the U_3O_7/U_4O_9 formation stage is to assume instant access of air to all grain boundaries followed by intragranular oxidation obeying parabolic kinetics. In such a scenario, the used fuel is deemed to be equivalent to a powdered sample having a particle-size distribution equal to the grain-size distribution of the used fuel. This will be realistic for most irradiated LWR fuels and will tend to overestimate rates (in terms of bulk conversion) in other cases.

The situation is more complex with the second stage of oxidation, from U_3O_7/U_4O_9 to U_3O_8. There is general agreement that this stage of the reaction follows nucleation-and-growth kinetics, but such a reaction can be difficult to model. Moreover, there is a wide range of reported values for the activation energy for U_3O_8 formation (Table 5); this introduces huge uncertainties in any extrapolative predictions of U_3O_8 formation rates. Examination of the reported activation energies has shown that many results are wrong because they do not properly deconvolute the first and second stages of oxidation, or because they do not recognize that the Arrhenius plot is not linear above $\sim$325°C. Critical review allowed us to narrow down the range of appropriate values for the activation energy, yielding a best estimate of 154 kJ mol^{-1}, which is applicable to temperatures below about 325°C. This is in good agreement with our own experimentally determined value (see below) for surface oxidation of unirradiated CANDU fuel [197]. We do not believe that there are any good estimates of the activation energy for the formation of U_3O_8 (specifically) on used fuel at low ($< \sim$325°C) temperatures.

Quantitative analysis of the kinetics for U_3O_8 formation is daunting because of the sigmoidal form of the reaction curve, which arises from the nucleation-and-growth mechanism. We have found that, in the case of unirradiated fuel, the surface oxidation can be modelled satisfactorily with Eq. (24) which can be approximated quite accurately by the first term alone:

$$\alpha = 1 - e^{-(\pi/3)\kappa t^3}, \tag{31}$$

where κ (h^{-3}) is related to absolute temperature (in K) by the expression

$$\ln \kappa = (-52{,}808 \pm 3.442)/T + 86.165. \tag{32}$$

The corresponding activation energy is 146 ± 10 kJ mol^{-1} (90% uncertainty limit) which is consistent with the results reported above for critical review of the literature data.

We emphasize that the model implied by the use of Eqs. (31) and (32) applies to *surface* oxidation (outermost ~ 1 μm) of *unirradiated* UO_2 fuel. Such a model is quantitative and reliable. It does not strictly apply to the three-dimensional case for bulk oxidation of used fuel during storage. However, the methodology presented herein is a useful conservative estimate of the rate of the three-dimensional oxidation reaction since U_3O_8 formation into the bulk of the sample will be somewhat less than unhindered oxidation along the surface. An example of predicted U_3O_8 formation kinetics is presented in Fig. 7. The following biases will apply to such calculations in the case of irradiated fuel.

(a) U_3O_8 formation is expected to be slower for irradiated fuels, i.e. κ is burnup dependent and probably decreases with increasing burnup. The dependence is not yet well quantified; however, calculations based on unirradi-

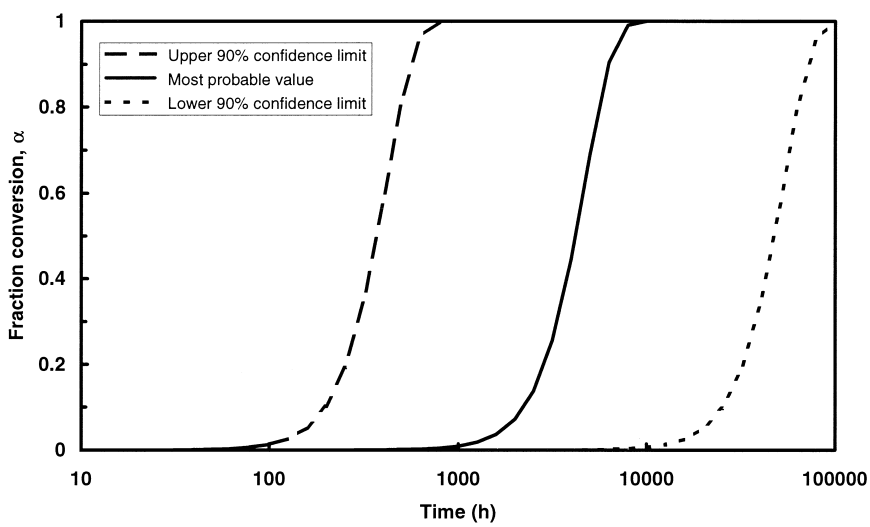

Fig. 7. Calculated extent of surface conversion of UO_2 to U_3O_8 in air at 200°C, in accordance with Eqs. (31) and (32).

ated fuel oxidation kinetic data may be regarded as conservative for irradiated fuel.

(b) Bulk formation of U_3O_8 is likely to be somewhat slower than surface oxidation, as discussed above.

(c) Nitrogen oxides, formed by radiolysis of air, may significantly accelerate U_3O_8 formation; this may reduce or negate the conservatism described in point (a). This phenomenon is not yet well quantified; preliminary estimates indicate that low concentrations of NO_2 may increase κ by about two orders of magnitude above the value for pure air oxidation at a given temperature [213].

(d) It has been assumed that grain-boundary oxidation is rapid relative to the rate of U_3O_8 formation; this is likely a good assumption for used LWR fuel, and is probably valid for used CANDU fuels for temperatures relevant to dry air storage.

6. Conclusions

The factors that affect the rate of oxidation of unirradiated UO_2 and of used fuel have been reviewed. Important issues relevant to the dry-air storage of used nuclear fuel have been identified, and areas requiring further study have been noted. The salient features of the study on the effect of various parameters on UO_2 oxidation include:

– Temperature: The predominant oxidation reaction varies from chemisorption (less than -130°C), through surface oxidation (-130 to ~ 100°C), to bulk formation of U_3O_7/U_4O_9 (~ 100 to ~ 250°C) and nucleation and growth of U_3O_8 (> 250°C).

– Moisture: Moist (e.g. $> 40\%$ RH) conditions lead to the formation of additional phases such as DS ($UO_3 \cdot \sim 0.8H_2O$). There appears to be a small, but significant, effect of relative humidity on the rate of oxidation of unirradiated UO_2; however, the effect of RH on the oxidation rate of used fuel is less clear and requires further study.

– Dopants: The presence of dopants such as Pu^{3+}, Th^{4+} or REE^{3+} as a solid solution in UO_2 results in enhanced stability of the cubic U_4O_{9+y} phase, but the reasons for this behaviour remain poorly understood.

– Oxygen partial pressure: Below ~ 13 kPa the oxygen pressure has a major influence on the rate of oxidation of UO_2 powders, but at higher pressures it has little, if any, effect. For sintered pellets, the rate of oxidation during the linear portion of the sigmoidal reaction curve increases with oxygen partial pressure, but the effect of pressure on the induction period, if any, is slight.

– NO_x: Radiolysis of nitrogen in the cover gas can lead to the formation of NO_x, which has a dramatic impact on both the rate and extent of oxidation. Despite its obvious practical importance, there is not yet a quantitative study relating the concentration of NO_x in the cover gas to the oxidation rate.

– Radiation: Gamma radiation has only a minor effect on the rate of oxidation (other than by generation of NO_x). The effects are most pronounced at low temperatures and for relatively defect-free material. The combination of gamma radiation and moisture appears to enhance the rate of UO_2 oxidation significantly.

– Aging: Storage in ambient air results in slower rates of oxidation, longer values of t_p, and powder formation at lower O/M ratios, relative to fresh samples. The reasons for such behaviour are not well understood but are perhaps related to the formation of a thin surface layer of highly oxidized material.

– Particle size: The oxidation behaviour of UO_2 varies from pyrophoric for extremely fine powders, to parabolic diffusion-controlled kinetics for powders, to sigmoidal nucleation-and-growth kinetics for sintered pellets.

– Grain size: For unirradiated UO_2, there is a negative correlation between grain size and the rate of oxidation during the induction period. Similar behaviour is observed for the linear rate of U_3O_8 formation but only for grain sizes below ~ 5 μm; above this size intragranular crack formation becomes rate determining.

– Density: Increased density is associated with decreased reactivity and longer induction times, especially for samples less than $\sim 95\%$ TD. It is often difficult to separate the effect of density from related fuel characteristics such as grain size, porosity, etc.

– Orientation effects: Crystal orientation appears to have only a slight effect on the rate of formation of U_3O_7/U_4O_9, but the effect is more significant for U_3O_8 growth.

It is generally accepted that the rate of formation of U_3O_7/U_4O_9 follows parabolic (diffusion-controlled) kinetics, although there has been disagreement as to whether the mechanism involves oxygen diffusion along a concentration gradient into UO_{2+x} or through a discrete layer of U_3O_7/U_4O_9 on the surface. Weight-gain experiments cannot distinguish between the two mechanisms, but the bulk of evidence (XRD, SEM) supports the discrete-layer mechanism.

The formation of U_3O_8 is a nucleation-and-growth process and kinetic data can be modelled effectively using either the Johnson-and-Mehl or the Avrami–Erofeev equations. However, the nucleation process is not yet well understood and the underlying factors that affect its rate (cracking, surface roughness) as well as the temperature-dependence of nucleation require further study to ensure that kinetic data obtained at high (> 200°C) temperatures are valid for temperatures relevant to the dry-air storage of used nuclear fuel (typically < 150°C).

Kinetic models for used fuel are more complex than for unirradiated UO_2 because of fast grain-boundary oxidation in the former, which leads to the rapid formation of U_3O_7/U_4O_9 and results in overlap between the first and second stages of oxidation. Models to describe the oxidation of UO_2 in defective fuel elements are thus complex

but have had some success. The general mechanism for UO_2 oxidation is well known and proceeds according to the reaction scheme in Eq. (12).

Some confusion persists over the possible involvement of an intermediate U_3O_7-type phase with $c/a \sim 1.015$. In contrast to the mechanism for unirradiated UO_2, used LWR fuel oxidizes via an intermediate that resembles U_4O_9 but which has a composition near $UO_{2.4}$. The structures of the various forms of U_3O_7 and U_4O_{9+y} have not yet been determined in detail.

Critical analysis of data reported in the literature has yielded estimates for the activation energy for the formation of U_3O_7/U_4O_9 on unirradiated UO_2 powders (96 kJ mol^{-1}) and sintered pellets (99 kJ mol^{-1}). Limited data for used fuel suggests that it has an activation energy of 106 kJ mol^{-1} for U_3O_7/U_4O_9 formation. The activation energy for the formation of U_3O_8 on unirradiated UO_2 has not yet been adequately studied. Various approaches have been used to estimate the activation energy for the formation of U_3O_8, but these involve assumptions about the relative rates of U_3O_8 nucleation and growth or use an approximation for the sigmoidal reaction kinetics. The best estimate of the activation energy for U_3O_8 formation below $\sim$325°C was calculated as 154 kJ mol^{-1}. Above $\sim$325°C the activation energy is somewhat lower [28]. For used fuel, there is no reliable estimate of the activation energy for U_3O_8 formation because of overlap between the first and second stages of oxidation. It is important to note that the activation energies for the formation of U_3O_8 represent an average for both the U_3O_8 nucleation and growth processes. Deconvolution of the oxidation kinetic data, so that individual rate expressions for nucleation and growth can be extracted, would be valuable in modelling the dry-air oxidation of used fuel.

The rate of formation of U_3O_7/U_4O_9 is between 2 and 50 times faster on used fuel than on unirradiated UO_2, partly because of the rapid rate of oxygen diffusion along grain boundaries in the former. By comparison, the rate of formation of U_3O_8 dominates the reaction kinetics above $\sim$300°C, and under these conditions used fuel and unirradiated UO_2 oxidize at approximately the same rate. It appears that there is a positive correlation between the time for U_3O_8 powder formation and burnup, at least for high burnups.

Acknowledgements

Part of the costs of this research were shared by the CANDU Owners Group (Working Party 40, WPIR No. 4001), under the participation of Ontario Hydro and AECL. The authors thank J.L. Crosthwaite, W.H. Hocking, D.W. Shoesmith, S. Sunder and K.M. Wasywich for critical review of this manuscript.

References

[1] S. Aronson, R.B. Roof Jr., J. Belle, J. Chem. Phys. 27 (1957) 137.
[2] M.J. Bannister, J. Nucl. Mater. 26 (1968) 174.
[3] J. Belle (Ed.), Uranium Dioxide: Properties and Nuclear Applications, Naval Reactors, Division of Reactor Development, USAEC, 1961.
[4] P.E. Blackburn, J. Weissbart, E.A. Gulbransen, J. Phys. Chem. 62 (1958) 902.
[5] K.T. Harrison, C. Padgett, K.T. Scott, J. Nucl. Mater. 23 (1967) 121.
[6] H.R. Hoekstra, A. Santoro, S. Siegel, J. Inorg. Nucl. Chem. 18 (1961) 166.
[7] H. Ohashi, H. Hayashi, M. Nabeshima, T. Morozumi, Bull. Fac. Eng. Hokkaido Univ. 134 (1987) 49.
[8] K.J. Schneider, S.J. Mitchell, A.B. Johnson Jr., Proc. 3rd Int. Conf. on High Level Radioactive Waste Management, Las Vegas, 1992, p. 1159.
[9] K.A. Simpson, P. Wood, Proc. NRC Workshop on Spent Fuel/Cladding Reaction During Dry Storage, Gaithersburg, MD, 1983 (NUREG/CP-0049), p. 70.
[10] P. Taylor, D.D. Wood, A.M. Duclos Mate, J. Nucl. Mater. 189 (1992) 116.
[11] S.R. Teixeira, K. Imakuma, J. Nucl. Mater. 178 (1991) 33.
[12] L.E. Thomas, R.E. Einziger, Mater. Charact. 28 (1992) 149.
[13] L.E. Thomas, O.D. Slagle, R.E. Einziger, J. Nucl. Mater. 184 (1991) 117.
[14] K.M. Wasywich, C.R. Frost, Proc. 2nd Int. Conf. on CANDU Fuel, Pembroke, Canada, 1989, p. 312.
[15] K.M. Wasywich, J.D. Chen, J. Freire-Canosa, S.J. Naqvi, Proc. 3rd Int. Spent Fuel Storage/Technology Symp./Workshop, Seattle, WA, 1986, p. 231.
[16] K.M. Wasywich, W.H. Hocking, D.W. Shoesmith, P. Taylor, Nucl. Technol. 104 (1993) 309.
[17] K.K. Bae, B.G. Kim, Y.W. Lee, M.S. Yang, H.S. Park, J. Nucl. Mater. 209 (1994) 274.
[18] T.K. Campbell, E.R. Gilbert, C.K. Thornhill, B.J. Wrona, Nucl. Technol. 84 (1989) 182.
[19] E.R. Gilbert, G.D. White, C.A. Knox, Proc. Int. Workshop On Irradiated Fuel Storage: Operating Experience and Development Programs, Toronto, Canada, 1984, p. 551.
[20] E.R. Gilbert, T.K. Campbell, C.K. Thornhill, G.F. Piepel, Proc. Workshop on Chemical Reactivity of Oxide Fuel and Fission Product Release, Berkeley, UK, 1987, p. 141.
[21] I.J. Hastings, D.H. Rose, J.R. Kelm, D.A. Irvine, J. Novak, J. Am. Ceram. Soc. 69 (1986) C16.
[22] K.S. Kim, G.S. You, D.K. Min, S.G. Ro, E.K. Kim, J. Korean Nucl. Soc. 29 (1997) 93.
[23] J. Novak, I.J. Hastings, E. Mizzan, R.J. Chenier, Nucl. Technol. 63 (1983) 254.
[24] D.J.M. Bevan, I.E. Grey, B.T.M. Willis, J. Solid State Chem. 61 (1986) 1.
[25] B.T.M. Willis, J. Chem. Soc. Faraday Trans. II 83 (1987) 1073.
[26] B.O. Loopstra, Acta Crystallogr. 17 (1964) 651.
[27] P. Taylor, D.D. Wood, A.M. Duclos, D.G. Owen, J. Nucl. Mater. 168 (1989) 70.
[28] D.G. Boase, T.T. Vandergraaf, Nucl. Technol. 32 (1977) 60.
[29] R.E. Einziger, J.A. Cook, Nucl. Technol. 69 (1985) 55.

[30] M. Guyonvarh, R. Le Meur, Report CEA-R-3329, 1967.
[31] EPRI, Electric Power Research Institute Report, EPRI NP-6387, 1989.
[32] S. Kawasaki, J. Nakamura, Proc. IAEA Coordinated Research Program Meeting on Behaviour of Spent Fuel and Storage Facility Components During Long-Term Storage, IAEA, Vienna, 1991.
[33] W. Jander, Z. Anorg. Allg. Chem. 163 (1927) 1.
[34] C. Wagner, K. Grunewald, Z. Phys. Chem. B40 (1938) 455.
[35] D.E.Y. Walker, J. Appl. Chem. 15 (1965) 128.
[36] G.-S. You, K.-S. Kim, S.-G. Ro, E.-K. Kim, Proc. JAERI-KAERI Joint Seminar on Post-Irradiation Examination, Oarai, Japan, 1992 (publ. 1993), JAERI-M 93-016, 1993, section 3.4.
[37] G.S. You, K.S. Kim, D.K. Min, S.G. Ro, E.K. Kim, J. Korean Nucl. Soc. 27 (1995) 67.
[38] W.A. Johnson, R.F. Mehl, Am. Inst. Mining and Metall. Eng., Metals Division, Tech. Publ. 1089, 1939.
[39] W.A. Johnson, R.F. Mehl, Trans. Am. Inst. Mining Metall. Eng. 135 (1939) 416.
[40] M. Avrami, J. Chem. Phys. 7 (1939) 1103.
[41] B.V. Erofeev, C. R. Acad. Sci. URSS 52 (1946) 511.
[42] P.M. Tucker, Proc. Workshop on Chemical Reactivity of Oxide Fuel and Fission Product Release, 1987, p. 49.
[43] T.K. Campbell, E.R. Gilbert, G.D. White, G.F. Piepel, B.J. Wrona, Nucl. Technol. 85 (1989) 160.
[44] P. Taylor, E.A. Burgess, D.G. Owen, J. Nucl. Mater. 88 (1980) 153.
[45] L.E. Thomas, R.E. Einziger, H.C. Buchanan, J. Nucl. Mater. 201 (1993) 310.
[46] B. Belbeoch, C. Piekarski, M.P. Perio, J. Nucl. Mater. 3 (1961) 60.
[47] L.E. Thomas, R.W. Knoll, L.A. Charlot, J.E. Coleman, E.R. Gilbert, Pacific Northwest Laboratory Report, PNL-6640, 1989, vol. 2.
[48] H.R. Hoekstra, S. Siegel, J. Inorg. Nucl. Chem. 18 (1961) 154.
[49] D.K. Smith, B.E. Scheetz, C.A.F. Anderson, K.L. Smith, Uranium 1 (1982) 79.
[50] P. Taylor, R.J. Lemire, D.D. Wood, Nucl. Technol. 104 (1993) 164.
[51] L.E.J. Roberts, J. Chem. Soc. (1954) 3332.
[52] I.F. Ferguson, J.D.M. McConnell, Proc. R. Soc. London Ser. A: 241 (1957) 67.
[53] J.S. Anderson, E.A. Harper, S. Moorbath, L.E.J. Roberts, UK Atomic Energy Authority Report, AERE C/R 886, 1955.
[54] J.S. Anderson, L.E.J. Roberts, E.A. Harper, J. Chem. Soc. (1955) 3946.
[55] L.E.J. Roberts, UK Atomic Energy Authority Report, AERE C/R 887, 1953.
[56] N. Cabrera, N.F. Mott, Rep. Prog. Phys. 12 (1949) 163.
[57] P.A. Tempest, P.M. Tucker, J.W. Tyler, J. Nucl. Mater. 151 (1988) 251.
[58] L.E. Thomas, R.E. Einziger, R.E. Woodley, J. Nucl. Mater. 166 (1989) 243.
[59] G.C. Allen, Philos. Mag. B 51 (1985) 465.
[60] S. Sunder, D.W. Shoesmith, M.G. Bailey, F.W. Stanchell, N.S. McIntyre, J. Electroanal. Chem. 130 (1981) 163.
[61] Hj. Matzke, Radiat. Eff. 64 (1982) 3.
[62] R. McEachern, J. Nucl. Mater. 245 (1997) 238.
[63] T. Smith, Atomics International Report, NAA-SR-4677, 1960.
[64] G.C. Allen, P.A. Tempest, J.W. Tyler, Philos. Mag. B 54 (1986) L67.
[65] D.R. McCracken, Atomic Energy of Canada Limited Report, AECL-8642, 1985.
[66] K.A. Peakall, J.E. Antill, J. Nucl. Mater. 2 (1960) 194.
[67] D.S. Cox, F.C. Iglesias, C.E.L. Hunt, N.A. Keller, R.D. Barrand, J.R. Mitchell, R.F. O'Connor, Proc. Symp. on Chemical Phenomena Associated With Radioactivity Releases During Severe Nuclear Plant Accidents, Anaheim, CA, 1986, p. 2–35.
[68] M. Iwasaki, T. Sakurai, N. Ishikawa, Y. Kobayashi, J. Nucl. Sci. Technol. 5 (1968) 652.
[69] I. Grenthe, J. Fuger, R.J.M. Konings, R.J. Lemire, A.B. Muller, C. Nguyen-Trung, H. Wanner, NEA-TDB: Chemical Thermodynamics of Uranium, NEA/OECD, North-Holland, Amsterdam, 1992.
[70] D.R. Olander, Nucl. Technol. 74 (1986) 215.
[71] P. Taylor, D.D. Wood, D.G. Owen, W.G. Hutchings, A.M. Duclos, Atomic Energy of Canada Limited Report, AECL-10476, COG-91-292, 1991.
[72] P. Taylor, D.D. Wood, D.G. Owen, G.-I. Park, J. Nucl. Mater. 183 (1991) 105.
[73] P. Taylor, D.D. Wood, D.G. Owen, J. Nucl. Mater. 223 (1995) 316.
[74] R.B. Gammage, E.L. Fuller Jr., H.F. Holmes, J. Phys. Chem. 74 (1970) 4276.
[75] M.L. Hair, Infrared Spectroscopy in Surface Chemistry, Marcel Dekker, New York, 1967, ch. 5.
[76] D.R. Olander, D. Sherman, M. Balooch, J. Nucl. Mater. 107 (1982) 31.
[77] S. Sunder, N.H. Miller, J. Nucl. Mater. 231 (1996) 121
[78] S. Sunder, N.H. Miller, Report AECL-11351 COG-95-296, 1995.
[79] J.K. Dawson, E. Wait, K. Alcock, D.R. Chilton, J. Chem. Soc. (1956) 3531.
[80] H.R. Hoekstra, S. Siegel, J. Inorg. Nucl. Chem. 35 (1973) 761.
[81] P.A.G. O'Hare, B.M. Lewis, S.N. Nguyen, J. Chem. Thermodyn. 20 (1988) 1287.
[82] R.J. Finch, M.L. Miller, R.C. Ewing, Radiochim. Acta 58&59 (1992) 433.
[83] S. Aronson, Bettis Technical Review, WAPD-BT-10 93, 1958.
[84] S.M. Lang, F.P. Knudsen, C.L. Fillmore, R.S. Roth, NBS Circ. 568 (1956).
[85] D.A. Vaughan, J.R. Bridge, C.M. Schwartz, Battelle Memorial Institute Report, BMI-1241, 1957.
[86] S.H. Huston, Mallinckrodt Chemical Works (USA) Report, NYO-5222, 1948.
[87] G.L. Martin, Mallinckrodt Chemical Works (USA) Report, NYO-5228, 1948.
[88] T.K. Campbell, E.R. Gilbert, C.K. Thornhill, G.D. White, G.F. Piepel, C.W.J. Griffin, Pacific Northwest Laboratories Report, PNL-6201, 1987.
[89] R. Wang, Pacific Northwest Laboratory Report, PNL-3566, 1981.
[90] T. Wadsten, J. Nucl. Mater. 64 (1977) 315.
[91] R.E. Einziger, H.C. Buchanan, Westinghouse Hanford Company Report, WHC-EP-0070, 1988.

[92] R.E. Einziger, R.E. Woodley, Proc. Waste Management '85, vol. 1, Tucson, AZ, 1985, p. 505.
[93] R.E. Woodley, R.E. Einziger, H.C. Buchanan, Nucl. Technol. 85 (1989) 74.
[94] C.R. Frost, K.M. Wasywich, Proc. Workshop on Chemical Reactivity of Oxide Fuel and Fission Product Release, Berkeley, UK, 1987, p. 319.
[95] K.M. Wasywich, C.R. Frost, Proc. 3rd Int. Conf. on High Level Radioactive Waste Management, Las Vegas, 1992, p. 1166.
[96] J.S. Anderson, D.N. Edgington, L.E.J. Roberts, E. Wait, J. Chem. Soc. (1954) 3324.
[97] J.S. Anderson, K.D.B. Johnson, J. Chem. Soc. (1953) 1731.
[98] S.F. Bartram, E.F. Juenke, E.A. Aitken, J. Am. Ceram. Soc. 47 (1964) 171.
[99] EURATOM, United States-Euratom Joint Research and Development Program Report, EURAEC-884, 1963.
[100] D.C. Hill, J. Am. Ceram. Soc. 45 (1962) 258.
[101] W.B. Wilson, C.A. Alexander, A.F. Gerds, J. Inorg. Nucl. Chem. 20 (1961) 242.
[102] R.J. Guenther, D.E. Blahnik, T.K. Campbell, U.P. Jenquin, J.E. Mendel, C.K. Thornhill, Pacific Northwest Laboratory Report, PNL-5109-106, UC-70, 1988.
[103] J. Janeczek, R.C. Ewing, J. Nucl. Mater. 190 (1992) 128.
[104] R.G.J. Ball, UK Atomic Energy Authority, Harwell Laboratory Report, AERE-R-13395, 1989.
[105] T. Fujino, C. Miyake, in: A.J. Freeman, C. Keller (Eds.), Handbook on the Physics and Chemistry of the Actinides, Vol. 6, Elsevier Science, Amsterdam, 1991, p. 155.
[106] F. Hund, U. Peetz, Z. Anorg. Allgem. Chem. 271 (1952) 6.
[107] C. Keller, Gmelins Handbuch der Anorganischen Chemie 8, Erganzungswerk, Band 55, Teil C3, Verlag Chemie, Weinheim/Bergstrasse, 1975, p. 197.
[108] T. Yamashita, Japan Atomic Energy Research Institute Report, JAERI-1310, 1988.
[109] H. Landspersky, M. Voboril, J. Inorg. Nucl. Chem. 29 (1967) 250.
[110] J. Rouault, J. Girardin, Proc. Workshop on Chemical Reactivity of Oxide Fuel and Fission Product Release, Berkeley, UK, 1987, p. 245.
[111] V.J. Tennery, T.G. Godfrey, J. Am. Ceram. Soc. 56 (1973) 129.
[112] M. Ishida, Y. Korei, J. Nucl. Mater. 210 (1994) 203.
[113] I. Cohen, R.M. Berman, J. Nucl. Mater. 18 (1966) 77.
[114] L.E.J. Roberts, L.E. Russell, A.G. Adwick, A.J. Walter, M.H. Rand, Proc. UN Conf. on the Peaceful Uses of Atomic Energy, 1959, p. 215.
[115] E.R. Gilbert, C.A. Knox, G.D. White, A.B. Johnson Jr., Am. Nucl. Soc. Trans. 50 (1985) 117.
[116] D.J. Wheeler, Proc. Workshop on Chemical Reactivity of Oxide Fuel and Fission Product Release, Berkeley, UK, 1987, p. 357.
[117] J.W. Choi, R.J. McEachern, P. Taylor, D.D. Wood, J. Nucl. Mater. 230 (1996) 250.
[118] P.G. Lucuta, R.A. Verrall, Hj. Matzke, B.J. Palmer, J. Nucl. Mater. 178 (1991) 48.
[119] D.N. Bykhovskii, M.A. Kuz'mina, G.S. Novikov, L.V. Solntseva, Radiokhimiya 34 (1992) 9.
[120] R.E. Einziger, H.C. Buchanan, L.E. Thomas, R.B. Stout, Proc. 3rd Int. Conf. on High Level Radioactive Waste Management, Las Vegas, 1992, p. 1449.
[121] J. Janeczek, R.C. Ewing, L.E. Thomas, J. Nucl. Mater. 207 (1993) 177.
[122] C. Sari, U. Benedict, H. Blank, Proc. Symp. on Thermodynamics of Nuclear Materials, IAEA, Vienna, 1968, p. 587.
[123] C.R.A. Catlow, Proc. R. Soc. London Ser. A: 353 (1977) 533.
[124] C.R.A. Catlow, J. Nucl. Mater. 79 (1979) 432.
[125] C.R.A. Catlow, A.B. Lidiard, Proc. 4th Symp. on Thermodynamics of Reactor Materials, vol. 2, IAEA, Vienna, 1975, p. 27.
[126] K. Park, D.R. Olander, High Temp. Sci. 29 (1990) 203.
[127] K. Park, D.R. Olander, J. Nucl. Mater. 187 (1992) 89.
[128] K.B. Alberman, J.S. Anderson, J. Chem. Soc. (1949) S303.
[129] E.H.P. Cordfunke, The Chemistry of Uranium, Elsevier, Amsterdam, 1969.
[130] H.R. Hoekstra, S. Siegel, F.X. Gallagher, J. Inorg. Nucl. Chem. 32 (1970) 3237.
[131] V.G. Vlasov, A.F. Bessonov, Izv. Vyssh. Ucheb. Zaved. Tsvetn. Metall. 5 (1962) 113.
[132] Y. Saito, Nihon Kinzoku Gakkai-shi 39 (1975) 760.
[133] V.D. Chumachkova, E.G. Lavut, K.M. Dunaeva, E.A. Ippolitova, Radiokhimiya 16 (1974) 548.
[134] J. Nakamura, T. Otomo, S. Kawasaki, J. Nucl. Sci. Technol. 30 (1993) 181.
[135] G.D. White, C.A. Knox, E.R. Gilbert, A.B. Johnson, Jr., Proc. NRC Workshop on Spent Fuel/Cladding Reaction During Dry Storage, Gaithersburg, MD, 1983 (NUREG/CP-0049), p. 102.
[136] A.H. Spellar, E.O. Maxwell, R.J. Pearce, Proc. BNES Conf. on Gas Cooled Reactors Today, vol. 4, Bristol, UK, 1982, p. 25.
[137] A.B. Johnson, Jr., E.R. Gilbert, D.R. Oden, D.L. Stidham, J.E. Garnier, D.L. Weeks, J.C. Dobbins, Proc. Waste Management '85, vol. 1, Tucson, AZ, 1985, p. 513.
[138] D.A. Dominey, J. Inorg. Nucl. Chem. 30 (1968) 1757.
[139] D.A. Dominey, H. Morley, D.A. Young, Trans. Faraday Soc. 62 (1966) 233.
[140] I.J. Hastings, J.A. Scoberg, K. Mackenzie, W. Walden, Atomic Energy of Canada Limited Report, AECL-6411, 1979.
[141] R.E. Einziger, S.C. Marschman, H.C. Buchanan, Nucl. Technol. 94 (1991) 383.
[142] M.E. Cunningham, J. Nucl. Mater. 187 (1992) 307.
[143] N. Nakae, A. Harada, T. Kirihara, S. Nasu, J. Nucl. Mater. 71 (1978) 314.
[144] N. Nakae, Y. Iwata, T. Kirihara, J. Nucl. Mater. 80 (1979) 314.
[145] W.J. Weber, Radiat. Eff. 83 (1984) 145.
[146] K. Nogita, K. Une, J. Nucl. Sci. Technol. 30 (1993) 900.
[147] K. Nogita, K. Une, J. Nucl. Sci. Technol. 31 (1994) 929.
[148] C.A. Colmenares, Prog. Solid State Chem. 9 (1975) 139.
[149] L.E.J. Roberts, Q. Rev. 15 (1961) 442.
[150] A. Bel, Y. Carteret, Proc. 2nd UN Int. Conf. on Peaceful Uses of Atomic Energy, vol. 6, 1958, p. 612.
[151] B.A.J. Lister, G.M. Gillies, Progress in Nuclear Energy, ser. 3, vol. 1, McGraw-Hill, New York, 1956, p. 19.
[152] V.A. Alekseyev, L.A. Anan'yeva, R.P. Rafal'skiy, Izv. Akad. Nauk SSSR Ser. Geol. 9 (1979) 80.
[153] H.R. Hoekstra, S. Siegel, Proc. Int. Conf. on the Peaceful Uses of Atomic Energy, vol. 7, Geneva, 1955 (publ. 1956), p. 394.

[154] S. Takeuchi, Y. Saito, Trans. Jpn. Inst. Metals (Sendai) 1 (1960) 1.
[155] C. Wagner, Z. Phys. Chem. B 21 (1933) 25.
[156] C. Wagner, Z. Phys. Chem. B 32 (1936) 447.
[157] H.S. Parker, S. Hasko, G.F. Rynders, C.H. Schreyer, H. Shapiro, H.J. Foster, S.T. DeLuca, U.S. National Bureau of Standards Report, NTIS-LAR-37, 1960.
[158] D. Kolar, E.D. Lynch, J.H. Handwerk, J. Am. Ceram. Soc. 45 (1962) 141.
[159] J.B. Price, M.J. Bennett, F.L. Cullen, J.F. Norton, S.R. Canetoli, Proc. 1st Int. Conf. on Microscopy of Oxidation, Cambridge, UK, 1991, p. 411.
[160] R.E. Einziger, L.E. Thomas, H.C. Buchanan, R.B. Stout, J. Nucl. Mater. 190 (1992) 53.
[161] R.E. Einziger and R.E. Woodley, Hanford Engineering Development Laboratory Report, HEDL-7556, WHC-EP-0107, Richland, WA, 1986.
[162] R.E. Einziger, R.E. Woodley, Proc. Workshop on Chemical Reactivity of Oxide Fuel and Fission Product Release, Berkeley, UK, 1987, p. 281.
[163] C. Araoz, Republic of Argentina, National Atomic Energy Commission Report, No. 74, 1962.
[164] P. Imris, J. Inorg. Nucl. Chem. 28 (1966) 99.
[165] V.V. Deshpande, R.P. Saxena, S.H. Daroowalla, M.D. Karkhanavala, Ind. J. Chem. 1 (1963) 511.
[166] R.J. Guenther, E.R. Gilbert, S.C. Slate, J.R. Devine, D.K. Kreid, W.L. Partain, Nucl. Eng. Int. 29 (363) (1984) 36.
[167] G.D. White, E.R. Gilbert, Proc. 3rd Int. Spent Fuel Storage/Technology Symp./Workshop, Seattle, WA, 1986, p. 147.
[168] P. Wood, G.H. Bannister, Proc. Workshop on Chemical Reactivity of Oxide Fuel and Fission Product Release, Berkeley, UK, 1987, p. 19.
[169] K.T. Scott, K.T. Harrison, Am. Nucl. Soc. Trans. 43 (1982) 317.
[170] G.C. Allen, P.A. Tempest, J.W. Tyler, J. Chem. Soc. Faraday Trans. I 84 (1988) 4049.
[171] G.C. Allen, P.A. Tempest, J.W. Tyler, J. Chem. Soc. Faraday Trans. I 84 (1988) 4061.
[172] J. Belle, B. Lustman, Westinghouse Electric Corporation Report TID-7546, Book 2, 1958, p. 442.
[173] G.C. Allen, P.A. Tempest, J.W. Tyler, Nature 295 (1982) 48.
[174] R.J. McEachern, P. Taylor, J. Nucl. Mater. 217 (1994) 322.
[175] G.C. Allen, P.A. Tempest, J.W. Tyler, J. Chem. Soc. Faraday Trans. I 83 (1987) 925.
[176] G.C. Allen, N.R. Holmes, Proc. Workshop on Chemical Reactivity of Oxide Fuel and Fission Product Release, Berkeley, UK, 1987, p. 1.
[177] F. Grønvold, J. Inorg. Nucl. Chem. 1 (1955) 357.
[178] B.E. Schaner, J. Nucl. Mater. 2 (1960) 110.
[179] E.F. Westrum Jr., F. Grønvold, J. Phys. Chem. Solids 23 (1962) 39.
[180] P. Pério, Bull. Soc. Chim. Fr. 20 (1953) 256.
[181] P. Pério, Bull. Soc. Chim. Fr. 20 (1953) 840.
[182] F. Grønvold, H. Haraldsen, Nature 162 (1948) 69.
[183] E.U. Kuz'micheva, L.M. Kovba, E.A. Ippolitova, Radiokhimiya 13 (1971) 852.
[184] A.F. Bessonov, V.N. Strekalovskii, V.M. Ust'yantsev, Kristallografiya 10 (1965) 570.
[185] A.F. Bessonov, G.A. Taksis, Y.N. Semavin, Izv. Akad. Nauk SSSR Neorg. Mater. 3 (1967) 1104.
[186] R.E. DeMarco, H.A. Heller, R.C. Abbott, W. Burkhardt, Am. Ceram. Soc. Bull. 38 (1959) 360.
[187] H. Ohashi, E. Noda, T. Morozumi, J. Nucl. Sci. Technol. 11 (1974) 445.
[188] P. Pério, doctoral dissertation, University of Paris, 1955.
[189] P. Pério, CEA, France, Report No. 363.
[190] J. Crank, The Mathematics of Diffusion, Clarendon, Oxford, 1956.
[191] G. Valensi, C. R. 202 (1936) 309.
[192] J.S. Kirkaldy, D.J. Young, Diffusion in the Condensed State, The Institute of Metals, London, 1987, p. 45.
[193] S. Whillock, J.H. Pearce, J. Nucl. Mater. 175 (1990) 121.
[194] Hj. Matzke, Diffusion Processes in Nuclear Fuels, in: R.P. Agarwala (Ed.), Diffusion Processes in Nuclear Materials, North Holland, Amsterdam, 1992, p. 35.
[195] J.S. Anderson, Bull. Soc. Chim. Fr. 20 (1953) 781.
[196] M. Avrami, J. Chem. Phys. 8 (1940) 212.
[197] R.J. McEachern, J.W. Choi, M. Kolar, W. Long, P. Taylor, D.D. Wood, J. Nucl. Mater. 249 (1997) 58.
[198] N.B. Hannay, Treatise on Solid State Chemistry, vol. 4, Reactivity of Solids, Plenum, New York, 1976.
[199] M.J. Bennett, J.B. Price, P. Wood, Nucl. Energy 27 (1988) 49.
[200] P. Wood, M.J. Bennett, M.R. Houlton, J.B. Price, Proc. BNES Conf., vol. 2, Stratford-upon-Avon, UK, 1985, p. 116.
[201] D.R. Olander, Adv. Ceram. 17 (1986) 271.
[202] R.B. Stout, H.F. Shaw, R.E. Einziger, Mater. Res. Soc. Symp. Proc. 176 (1990) 475.
[203] F. Garisto, Atomic Energy of Canada Limited Report, AECL-10734, COG-92-311, 1993.
[204] M. Kolar, Atomic Energy of Canada Limited Report, AECL-11174, COG-I-94-446, 1995.
[205] R.E. Woodley, R.E. Einziger, H.C. Buchanan, Westinghouse Hanford Company Report, WHC-EP-0107, 1988.
[206] H.E. Kissinger, Anal. Chem. 11 (1957) 1702.
[207] R.E. Einziger, R.V. Strain, Proc. Int. Workshop on Irradiated Fuel Storage: Operating Experience and Development Programs, Toronto, Canada, 1984, p. 599.
[208] A.R. West, Solid State Chemistry and its Applications, John Wiley and Sons, New York, NY, 1985.
[209] I.J. Hastings, J. Novak, Proc. NRC Workshop on Spent Fuel/Cladding Reaction During Dry Storage, Gaithersburg, MD, NUREG/CP-0049, 1983, p. 26.
[210] L.E. Thomas, J.M. McCarthy, E.R. Gilbert, Proc. 3rd Int. Spent Fuel Storage/Technology Symp./Workshop, CONF-860417, Seattle, WA, 1986, p. W-40.
[211] C.S. Olsen, EG&G Idaho, Report, NUREG/CR-4074, EGG-2364, 1985.
[212] C.S. Olsen, Nucl. Eng. Design 89 (1985) 51.
[213] R.J. McEachern, S.Sunder, P. Taylor, D.C. Doern, N.H. Miller, D.D. Wood, The influence of nitrogen dioxide on the oxidation of UO_2 in air at temperatures below 260°C, J. Nucl. Mater., in press.